HAL open science

Hepatic inflammation elicits production of proinflammatory netrin-1 through exclusive activation of translation

Romain Barnault, Claire Verzeroli, Carole Fournier, Maud Michelet, Anna Rita Redavid, Ievgeniia Chicherova, Marie-laure Plissonnier, Annie Adrait, Olga Khomich, Fleur Chapus, et al.

To cite this version:

Romain Barnault, Claire Verzeroli, Carole Fournier, Maud Michelet, Anna Rita Redavid, et al.. Hepatic inflammation elicits production of proinflammatory netrin-1 through exclusive activation of translation. Hepatology, 2022, 76 (5), pp.1345-1359. 10.1002/hep.32446 . hal-03864005

HAL Id: hal-03864005

https://hal.science/hal-03864005v1

Submitted on 7 Jun 2023

HAL is a multi-disciplinary open access archive for the deposit and dissemination of scientific research documents, whether they are published or not. The documents may come from teaching and research institutions in France or abroad, or from public or private research centers.

L'archive ouverte pluridisciplinaire **HAL**, est destinée au dépôt et à la diffusion de documents scientifiques de niveau recherche, publiés ou non, émanant des établissements d'enseignement et de recherche français ou étrangers, des laboratoires publics ou privés.

Hepatic inflammation elicits production of proinflammatory netrin-1 through exclusive activation of translation

Romain Barnault[1#], Claire Verzeroli[1#], Carole Fournier[2], Maud Michelet[1], Anna Rita Redavid[3], Ievgeniia Chicherova[1], Annie Adrait[4], Olga Khomich[1], Fleur Chapus[1], Mathieu Richaud[1], Federica Grazia Centonze[5], Julie Lucifora[1], Birke Bartosch[1], Michel Rivoire[6], Hesso Farhan[5], Yohann Couté[4], Valbona Mirakaj[7], Thomas Decaens[2], Patrick Mehlen[3], Benjamin Gibert[3], Fabien Zoulim[1,8], Romain Parent[1*]

[1] Pathogenesis of Chronic Hepatitis B and C laboratory - LabEx DEVweCAN, Inserm U1052, Cancer Research Centre of Lyon, F-69003 Lyon, France, University of Lyon, F-69003 Lyon, University of Lyon 1, ISPB, Lyon, F-69622, France, CNRS UMR5286, F-69083 Lyon, France, Centre Léon Bérard, F-69008 Lyon, France

[2] Institute for Advanced Biosciences, Inserm U1209, University of Grenoble-Alpes, F-38700 La Tronche, France

[3] Apoptosis, Cancer and Development Laboratory - LabEx DEVweCAN, Inserm U1052, Cancer Research Centre of Lyon, F-69003 Lyon, France, University of Lyon, F-69003 Lyon, University of Lyon 1, ISPB, Lyon, F-69622, France, CNRS UMR5286, F-69083 Lyon, France, Centre Léon Bérard, F-69008 Lyon, France

[4] University of Grenoble-Alpes, Inserm, CEA, UMR BioSanté U1292, CNRS CEA FR2048, F-38000, Grenoble, France

[5] Institute of Basic Medical Science, University of Oslo, N-0372, Oslo, Norway

[6] Léon Bérard Cancer Center, F-69008 Lyon, France, Université Lyon 1, Lyon, F-69622, France

[7] Department of Anesthesiology and Intensive Care Medicine, University Hospital Tübingen, Eberhard-Karls-University, DE-72076, Tuebingen, Germany.

[8] Hospices Civils de Lyon, Service of hepato-gastroenterology, F-69001 Lyon, France

[#] Equal contributions

* Corresponding author

Abstract

Causal links between inflammation and cancer are well-established, and research into the means of controlling the former is paramount. Netrin-1 is targeted in clinical trials as it displays pro-tumoral properties in inflammatory contexts in some organs, which led us to investigate its status with respect to inflammation in the liver. Here, based on a positive clinical correlation between netrin-1 levels and inflammation, experimentally confirmed in mice by inducing inflammation using poly(I:C) as a TLR3 agonist, we identify netrin-1 as a hepatic inflammation-inducible factor and decipher its underlying mechanism. Surprisingly, netrin-1 upregulation relied on a hitherto unknown mode of induction, namely its exclusive translational activation following the transfer of *NTN1* to the ER, ruling out any other traditional processes through exhaustive approaches. Our *in vitro* approaches unveiled a direct interaction between the Staufen-1 protein and netrin-1 mRNA, and were further validated in mice. Based on these findings, we finally explored the impact of a phase 2 clinical trial-validated humanized anti-netrin-1 antibody (NP137) on mice livers, and observed a clear anti-inflammatory activity. Hence, our results provide a better understanding of the interplay between inflammation and chronic liver disease and offer an innovative therapeutic perspective for interfering with their adverse evolution.

Introduction

Chronic liver diseases (CLDs) represent the main etiological conditions for the onset of liver injury, cirrhosis, and hepatocellular carcinoma (HCC) [1]. Though CLDs exhibit a high degree of diversity in terms of causal effects, ranging from infectious (hepatitis B and C viruses, HBV and HCV), to metabolic, to toxic and finally genetic, they all converge towards hepatic inflammation. This response in turn drives hepatocytic turnover, extracellular matrix accumulation, histological worsening and the long-term induction of carcinogenic mediators eventually leading to the development of HCC [2]. A clear understanding of the outcome of this inflammatory response and of its onset in the hepatic tissue is hampered by biologically opposite functions, as it favors viral and dead cell clearance, as well as histological wound healing, but exacerbates fibrogenesis, thus inducing cirrhosis and oncogenesis. Hence, the identification of factors involved in a harmful regulation of inflammation may lead to its clinical improvement.

We previously documented the pathogenic implication of netrin-1, a developmentally-regulated and secreted factor of neural origin [3], in liver diseases. Indeed, we showed that the expression of this factor is reactivated in several illnesses in adulthood, including several types of carcinomas [4-7] and also induced by HBV and HCV [8, 9]. Netrin-1 is well-known for preventing cellular apoptosis through its binding to ‘dependence receptors’ [5, 6, 10-15], and we demonstrated that it endowed hepatocytes with resistance to apoptosis during the unfolded protein response (UPR) [16], a hallmark of CLDs and cirrhosis [17-19]. Owing to the causal link between inflammation, cancer in general, and HCC, we hypothesized that hepatic inflammation and netrin-1 may be reciprocal influencers in the liver.

Owing to conflicting data on the implication of netrin-1 in inflammation, by either exacerbating [20-22] or dampening [23-25] the inflammatory response according to the chronic inflammation setting studied, we conducted extensive mechanistic experiments to document its implication in this organ, similarly to that described in inflammatory bowel disease and colorectal cancer [6, 26]. We first confirmed a clinical correlation between inflammation and netrin-1 upregulation in a cohort of HBV samples, which we then validated in mice using poly(I:C) to induce inflammation. Through a series of experiments on HepaRG cells and PHH, including polysomal isolation and fractionation, SILAC metabolic incorporation, and direct interaction assays, we dissected each step of netrin-1 biogenesis to comprehend its induction. We unveiled the implication of the Staufen-1 protein in netrin-1 mRNA localization at the ER, fostering its translation activation and identified distinct yet converging mechanisms in both hepatocytic environments. Finally, we confirmed these data in mice through netrin-1 capture experiments using a phase I and II clinical trial-validated (NCT02977195) humanized antibody [27] that reversed hepatic inflammation *in vivo*. Hence, we show that netrin-1 is a newly identified

38 hepatic inflammation-inducible factor endowed with pro-inflammatory properties, and that an
39 antibody enabling netrin-1 capture may dampen hepatic inflammation, a dataset of general
40 interest in CLD.

Material and methods

Clinical samples

Clinical liver samples were used under the French IRB 'CPP South-East IV' approval #A16/207 (2016) related to the Inserm unit 1052 Hepatology biobank, France (#DC2008-235). Written informed consent was obtained from each patient and conformed to the ethics guidelines of the 1975 Declaration of Helsinki. Sample characteristics are shown in the **Suppl. Table 1.** All activity scores were determined by the pathology department of the Lyon University Hospital using standardized procedures.

Animal housing, treatment and sample harvest

All trials were performed under IRB agreement #CECCAP_CLB_2014_015 as previously described (doi 10.15252/emmm.202012878). Eight-week-old C57BL/6J mice (Janvier Laboratories, Saint Berthevin, France) were injected intraperitoneally with poly(I:C) (Invivogen, Toulouse, France) at indicated doses or PBS for 16 h and sacrificed prior to liver harvest. Due to liver zonation considerations [28], all analyses were performed after selection on ice of the median hepatic lobe of all animals. Hepatic lobe samples were immediately snap frozen in liquid nitrogen and subsequently thawed on ice prior to homogenization using a Dounce apparatus previously refrigerated, followed by the addition of RIPA or polysome buffer (see below, protein or polysome-related studies) or Trizol (see below, total RNA-related studies, Invitrogen).

Immunohistochemistry

For histological examination, tissue samples were fixed in 10% buffered formalin and embedded in paraffin, and prepared according to conventional procedures. Immunohistochemistry was performed on an automated immunostainer (Ventana Discovery XT, Roche, Meylan, France) using the Discovery HRP Kit according to the manufacturer's instructions. Sections were incubated with an anti-netrin-1 antibody (1/500; see **Suppl. Table 2**). Staining was visualized with DAB solution with 3,3′-diaminobenzidine as a chromogenic substrate. Finally, the sections were counterstained with Gill's hematoxylin.

Flow cytometry analysis

Pieces of liver were minced and digested in RPMI-1640 supplemented with mouse tumor dissociation enzymes (Miltenyi Biotec, Bergisch Gladbach, Germany) for 40 min at 37°C. Digested samples were filtered through a 70 µm nylon mesh to obtain uniform single-cell suspensions. Cells were washed with complete RPMI medium containing 10% decomplemented FBS, 1% NEAA, 1% Sodium Pyruvate and 1% Penicillin-Streptomycin

78 (Gibco™) and resuspended in 500 µL of Flow Cytometry Staining Buffer (FCSB)
79 (eBioscience™). 100 µL of cell suspension was used for staining in U-shaped 96-well plates.
80 After PBS 1X washing, cells were stained with LIVE/DEAD™ Fixable Red Dead Cell Stain Kit
81 for 30 min protected from light at room temperature. Fc receptors were blocked with anti-
82 CD16/CD32 (TruStain FcX™; Biolegend) and cells were stained for cell surface antigens (see
83 **Suppl. Table 2**). For intracellular staining, cells were fixed and permeabilized using the Foxp3
84 / Transcription Factor Staining Buffer Set (eBioscience™). Events were acquired on a BD-
85 LSRII flow cytometer (BD Biosciences, Le Pont-De-Claix, France), collected with the BD
86 FACSDiva 6.3.1 software and analyzed using Flowjo (or Flowlogic) software.
87
88 **Cell culture and siRNA/plasmids transfection**
89 Cells were grown in a 5% CO_2 humidified atmosphere at 37°C. All reagents pertaining to
90 HepaRG cell culture were purchased from ThermoFischer Scientific (Les Ulis, France) unless
91 otherwise indicated. HepaRG cells were seeded at a density of $4.10^4/cm^2$ in William's E
92 medium containing insulin 5 mg/mL, penicillin 100 IU/mL, streptomycin 100 mg/mL, and 10%
93 fetal bovine serum (Hyclone, Illkirch, France). The medium was supplemented with
94 hydrocortisone hemisuccinate at a concentration of 5.10^{-5} mol/L (Pharmacia Upjohn,
95 Guyancourt, France). Medium was renewed twice a week. siRNAs (Flexitube, Qiagen, Les
96 Ulis, France, **Suppl. Table 3**) and plasmids were transfected using RNAiMax (Thermo, Les
97 Ulis, France) or Mirus LT1 reagents (Mirus-Bio, Euromedex, Souffelweyersheim, France),
98 following the manufacturer's procedures at a final concentration of 10 nM and 1 µg/mL,
99 respectively. All transfections were performed in suspension before distribution in wells and
100 poly(I:C) treatment in order to prevent transfection yield variability. Primary human hepatocytes
101 (PHHs) were isolated from surgical liver resections, after informed consent of patients (IRB
102 agreements #DC-2008-99 and DC-2008-101) as previously described [29] and cultured in
103 complete William's medium supplemented with 1.8% DMSO (Sigma, St Quentin, France). All
104 PHH-related data were obtained from at least three distinct patients. For TLR3-specific or pan-
105 TLR stimulation, cells were treated with Pam3-CSk4, LPS, FLA, FSL, Riboxol and LMW or
106 HMW poly(I:C) (InvivoGen, Toulouse, France) three to four days after seeding (*i.e.* after having
107 reached confluency) for the indicated time points and/or concentrations.
108
109 **Cell viability assays**
110 The Neutral Red (NR) assay was conducted as described by Repetto [30]. Briefly, the NR
111 stock solution (40 mg NR dye in 10 mL PBS) was diluted in culture medium to a final
112 concentration of 4 mg/mL and then centrifuged at 600*g* for 10 min to remove any precipitated
113 dye crystals. Cells were then incubated with 100 µL of NR medium for 1 h. NR medium was
114 removed and the cells washed with PBS. Plates were incubated for 10 min under shaking with

115 150 µL/well of NR destain solution (50% ethanol 96%, 49% deionized water, 1% glacial acetic
116 acid). OD at 540 nm was measured.
117
118 **Western blotting**
119 Immunoblotting was performed using 40 µg of RIPA (50 mM Tris HCl (pH 8.0), 150 mM NaCl,
120 1% NP-40, 0.5% sodium deoxycholate, 0.1% SDS, 10 mM sodium fluoride, 50 mM
121 orthovanadate, 1x protease inhibitor cocktail (Roche))-processed cell lysates, then resolved
122 on 8% or 10% SDS-PAGE, blotted onto nitrocellulose membranes (Amersham Biosciences),
123 blocked using 5% low fat dried milk in TBS Tween 0.1% for 1 hour at RT and probed overnight
124 at 4°C with corresponding antibodies listed in the **Suppl. Table 2**. After three washes in PBS-
125 Tween 0.1%, membranes were incubated for 1 h at room temperature with secondary
126 antibodies coupled to HRP (1/5,000, Sigma-Aldrich, St-Quentin, France) prior to
127 chemiluminescence-based revelation using the Clarity Western ECL substrate (Bio-Rad,
128 Versailles, France). The Western blot specificity of the netrin-1 antibody was extensively
129 verified in-house prior to conducting experiments (**Suppl. Fig. 1**).
130
131 **Immunofluorescence**
132 Cells were fixed in -20°C methanol/acetone after one wash of ice-cold PBS, blocked in 5%
133 goat serum (Eurobio, Les Ulis, France) at room temperature for 15 min, incubated overnight
134 with corresponding antibodies listed in **Suppl. Table 2** in PBS/0.1% Triton X-100, washed prior
135 to incubation with secondary antibodies listed in the **Suppl. Table 2**, mounted with DAPI. Cells
136 were finally visualized under a confocal microscpoe (Leica SP5X, magnification 63X, Zoom =
137 2).
138
139 **Netrin-1 immunoprecipitation**
140 For netrin-1 immunoprecipitation from tissue culture medium, serum-free medium
141 complemented or not with heparin (2 µg/mL, Sigma-Aldrich, France), was applied to the cells
142 overnight, 60 h after poly(I:C) treatment. 5x or 1x lysis buffer (20 mM Tris pH 7.5, 150 mM
143 NaCl, 1 mM EDTA, 1 mM EGTA, 0.1% Triton X-100, Protease inhibitor cocktail 1x) were used
144 for supernatant or total lysates immunoprecipitation, respectively. Two µg of anti-netrin-1
145 NP137 antibody [27] / 5 mL of medium or 2 µg NP137 / mg of protein extracted from total
146 lysates were incubated overnight on a rotating wheel at 4°C. Twenty µL of SureBeads™
147 Protein A Magnetic Beads (Biorad) was added for 2µg of antibody, for 1 h on a rotating wheel
148 at 4°C. Beads were then washed three times with lysis buffer 1x and eluted in 20 µL of 1x
149 Laemmli buffer for 5 min at 95°C (Staufen-1, Netrin-1 IP) or extracted with acid phenol
150 (Invitrogen) reagent followed by proteinase K extraction (Staufen-1 IP) as described earlier
151 [31].

152

153 **Total RNA extraction and RT-qPCR**

154 Total RNA was extracted using Trizol (Invitrogen). One µg of RNA was DNAse I-digested
155 (Promega, Charbonnières, France) and then reverse transcribed using MMLV reverse
156 transcriptase (ThermoFischer) according to the manufacturer's instructions. Pre-mRNA-
157 targeting qPCR was tested for absence of DNA-based qPCR signal upon heat inactivation of
158 MMLV. Quantitative real-time PCR was performed on 1/5th diluted samples on a LightCycler
159 96 device (Roche, Meylan, France) using the low Rox qPCR mix (Bioline, Paris, France). PCR
160 primer sequences (5′-3′) and qPCR conditions are listed in the *ad hoc* section. Specificity of all
161 primers (**Suppl. Table 4**) was assessed by melting curve analyses and agarose gel
162 electrophoresis. Performance of all primers was quantified using serial 3-fold dilutions of target
163 templates.

164

165 **Nascent RNA capture**

166 Cells were treated with 0.2 mM ethynyl uridine (EU) for 24 h in order to obtain nascent RNAs
167 with an incorporated EU label. Total RNAs were isolated with Tizzol (Invitrogen). The EU-
168 labeled RNAs were biotinylated and captured using the Click-it Nascent RNA Capture Kit (Life
169 Technologies), in accordance with the manufacturer's instructions. One µg of total RNA was
170 used for biotinylation with 0.25 mM biotin azide in the Click-iT reaction buffer. The RNAs were
171 precipitated with ammonium acetate and ethanol and resuspended in UltraPure water. EU-
172 labeled biotinylated RNAs were captured using Dynabeads MyOne Streptavidin T1 magnetic
173 beads. 0.5 µg of biotinylated RNAs was mixed with Click-iT RNA binding buffer and heated at
174 68°C for 5 min, followed by the addition of the beads (25 µL of suspension per reaction) and
175 incubation at room temperature for 30 min while gently vortexing. The beads were immobilized
176 using the DynaMag-2 magnet and were washed with Click-iT washing buffers 1 and 2. The
177 washed beads were resuspended in Click-iT wash buffer 2 and used for cDNA synthesis.

178

179 **Sequential extraction**

180 This protocol followed Stephens et al. [32, 33] using the following buffer compsitions.
181 Permeabilization: 110mM KOAc, 25mM KHEPES pH7.2, 2.5mM Mg(OAc)2, 1 mM EGTA,
182 0.015% digitonin, 1 mM DTT, 1 mM PMSF, 200µM VRC. Wash: 110 mM KOAc, 25 mM
183 KHEPES pH 7.2, 2.5 mM Mg(OAc)2, 1 mM EGTA, 0.004% digitonin, 1 mM DTT, 1 mM PMSF,
184 200µM VRC. Lysis: 400 mM KOAc, 25 mM KHEPES pH 7.2, 15 mM Mg(OAc)2, 1% (v/v) NP-
185 40, 0.5% (w/v) DOC, 1 mM DTT, 1 mM PMSF, 200µM VRC. Briefly, aspiration of medium and
186 washing of cells (100 mm Petri dishes) with 5-10 mL ice-cold PBS to remove any excess
187 culture medium was first conducted. Flasks were then gently coated with digitonin-containing
188 1 mL permeabilization buffer and shaken at 4°C on ice for 5 min. At this point, loss of plasma

189 membrane and soluble cytosolic contents could be observed using phase contrast microscopy
190 (**Suppl. Fig. 2A**). The flasks were then straightened (vertical position) and the buffer allowed
191 to drain for 1 min. The soluble material (cytosol) was transferred to a 1.5 mL microcentrifuge
192 tube on ice, before gently washing the flasks with 5 mL of digitonin-free wash buffer, which
193 was then discarded. The flasks were next coated with 1 mL of NP40-containing lysis buffer
194 and shaken on ice for 5 min. At this point, only nuclei and insoluble cytoskeletal components
195 remain attached to the culture flask, which once again could be visualized using routine phase
196 contrast microscopy (**Suppl. Fig. 2B**). The flasks were subsequently straightened and the
197 buffer allowed to drain for 1 min. The resulting soluble (membrane-bound) material was
198 transferred to a 1.5 mL microcentrifuge tube. Finally, soluble lysates were clarified at 10,000*g*
199 for 10 min at 4°C and the supernatants transferred to new tubes.
200
201 **Polysome isolation and profiling**
202 For polysome fractionation, cycloheximide (Sigma, 100µg/ml; Interchim, Montluçon, France)
203 was added to the medium for 5 and/or 15 min, prior to harvesting. The medium was then
204 removed and the cells washed with ice-cold PBS containing 100 µg/mL cycloheximide. The
205 cells were then scraped, centrifuged at 800*g* for 5 min at 4°C and cytoplasmic RNA was
206 obtained by lysis (20 strokes of a p1000 pipet) of the cell pellet in 1 mL of polysome buffer
207 containing 10 mM Tris-HCl (pH 8.0), 140 mM NaCl, 1.5 mM MgCl2, 0.5% Nonidet P-40, and
208 40 mM vanadyl ribonucleoside complexes (VRC), 100 µg/mL cycloheximide (CHX), 20 mM
209 dithiothreitol (DTT), and 1 mM phenylmethanesulfonyl fluoride (PMSF), all reagents were
210 supplied by Sigma. Mitochondria and membrane debris were removed by centrifugation
211 (10,000*g*, 5 min, 4°C). The post-mitochondrial supernatants were overlaid onto a 15-40%
212 sucrose gradient and spun at 38,000rpm for 2 h at 4°C in a SW41Ti rotor (Beckman Coulter,
213 Fullerton, CA, USA). Fractions were collected from the top of each gradient using a 240 nm
214 UV reader-coupled fraction collector (Brandel, Glasgow, UK). Free mRNPs, monosomes and
215 polysomes were located through the interpretation of UV gradient traces. RNA extraction was
216 done using the acid phenol approach detailed previously [8].
217
218 **Mass spectrometry-based proteomic analyses**
219
220 The gel bands containing immunocaptured netrin-1 from the three independent experiments
221 were cut and digested in-gel using trypsin (modified, sequencing purity, Promega), as
222 previously described [34]. The resulting peptides were analyzed by online nanoliquid
223 chromatography coupled to MS/MS (Ultimate 3000 RSLCnano and Q-Exactive HF, Thermo
224 Fisher Scientific) using a 60 min gradient. For this purpose, the peptides were sampled on a
225 pre-column (300 µm x 5 mm PepMap C18, Thermo Scientific) and separated in a 75 µm x 250

226 mm C18 column (Reprosil-Pur 120 C18-AQ, 1.9 µm, Dr. Maisch). The MS and MS/MS data
227 were acquired by Xcalibur (Thermo Fisher Scientific).
228 Peptides and proteins were identified and quantified using MaxQuant (version 1.6.17.0) [35]
229 using the Uniprot database (*Homo sapiens* taxonomy, May 2020 version) and the frequently
230 observed contaminant database embedded in MaxQuant. Trypsin was chosen as the enzyme
231 and two missed cleavages were allowed. Peptide modifications allowed during the search
232 were: carbamidomethylation (C, fixed), acetylation (Protein N-ter, variable) and oxidation (M,
233 variable). Minimum peptide length and minimum number of unique peptides were set at seven
234 amino acids and one, respectively. Maximum false discovery rates - calculated by employing
235 a reverse database strategy - were set at 0.01 of the peptide-spectrum match, peptide and
236 protein levels. The netrin-1 ratio in heavy over medium forms (replicates 1 and 3) or medium
237 over heavy forms (replicate 2) were calculated for each replicate based on the corresponding
238 peptide ratios.
239
240 **CLIP assay**
241 Poly(I:C) treated and mock cells were supplemented with 100 µg/mL cycloheximide (5 min.
242 37°C), then washed with ice-cold PBS, fixed under UV light (0.2 J/cm^2), scraped with ice-cold
243 PBS, spun down at 1,000*g* for 5 min at 4°C and snap-frozen in liquid nitrogen. Cells were
244 subsequently lysed in a buffer composed of 20 mM Tris pH 7.5, 150 mM NaCl, 1 mM EDTA,
245 1 mM EGTA, 0,1% NP40, Protease inhibitor cocktail 1x, RNAse Out 100 U/mL, and 400 µM
246 VRC. The 35 strokes of Dounce homogenizer were applied to the sample before clarification
247 at 5,000*g* for 5 min at 4°C. After preclearing using naked protein A-coated magnetic beads
248 (Bio-Rad #161-4013), 2 µg of IgG control or anti-Staufen antibody (**Suppl. Table 3**) was mixed
249 to 0.5 mg of lysates overnight under rotating incubation at 4°C. Beads were then added to
250 complexes and incubated on a rotating wheel at 4°C for 2 h, then washed twice with lysis
251 buffer. Twenty µg of total lysates 1/6th of the IP fraction, as well as flow-through fractions were
252 loaded onto SDS-PAGE gels for subsequent immunodetection of the proteins of interest.
253 Staufen-1-bound RNA extraction was conducted using the acid phenol approach detailed
254 previously [8]. Bound RNAs were retrotranscribed using the Superscript IV Vilo RT enzyme
255 (Invitrogen) and corresponding cDNAs were amplified using the Bioline No-Rox qPCR kit.
256
257 **Filter binding assay**
258 The *NTN1* 5'UTR was *in vitro* transcribed using the MEGAscript™ T7 Transcription Kit,
259 (Ambion, #AMB13345) and then biotinylated (Pierce™ RNA 3' End Biotinylation Kit, Thermo
260 #20160). HBV RNA epsilon loop was chemically synthesized and labeled (Genscript,
261 Piscataway, USA). Sequences and genetic references are provided in **Suppl. Table 5.** RNA
262 renaturation was performed by heating samples at 95°C for 5 min before slowly cooling to

263 room temperature. RNA constructs (0.1 nM) were then incubated with increasing
264 concentrations of the purified recombinant Staufen-1 protein (Origen, #TP760787; 0-100 nM)
265 in binding buffer (Tris-HCl, pH 7.4, 20 mM; K(AcO), 100 mM; KCl, 200 mM; $Mg(AcO)_2$, 2.5 mM;
266 DTT, 1 mM) for 30 min at 37 °C. The reactions were then loaded onto a filter sandwich
267 composed of 0.45 µm nitrocellulose filters (GE Healthcare Life Science) located above nylon
268 filters (GE Healthcare Life Science). Both membranes were pre-soaked in binding buffer and
269 assembled in a dot-blot apparatus. Samples were directly added to the filters under vacuum
270 and subsequently washed twice with 400 µL of ice-cold binding buffer while a vacuum was
271 being applied. Both membranes were then UV crosslinked (0.12 J/cm^2). Signal development
272 was performed using the Chemiluminescent Nucleic Acid Detection Module Kit, thermo
273 #89880. Quantification of the obtained signals was done using Image Lab. Kd values were
274 calculated using the Sigma Plot 8.02© software according to the equation
275 $y = y0 + (B_{max} \cdot xn)/(K_d^n + x^n)$, where y is the percentage of complexed RNA, Bmax is the binding
276 yield, x is the concentration of the target RNA, Kd is the dissociation constant and n is the Hill
277 coefficient.
278
279 **RUSH assay**
280 HepaRG cells transfected with a GFP-tagged A_1AT RUSH reporter described previously [36]
281 were treated or not with poly(I:C). After 72 h, cells were treated with 40 µM biotin and then
282 fixed with 3% paraformaldehyde at different time points. After immunofluorescence staining,
283 images were acquired on a Leica SP5 confocal laser scanning microscope using the 63× oil
284 objective at two-fold magnification.
285
286 **Netrin-1 Crispr cell lines**
287 A netrin KO Crispr cell line and its ad hoc control cell line were generated.
288 The Zhang lab protocol [37] was used. Briefly, guide sequences (**Suppl. Table 6**) were
289 inserted into lentiCRISPR v2 (Addgene plasmid #52961) and lentiCRISPR v2-Blast (Addgene
290 plasmid #83480). DNAs (Gag-Pol + Env + lentiCRISPRv2 or lentiCRISPRv2 Blast) were
291 transfected into 2×10^6 HEK293T cells (ATCC CRL-1573) seeded the day before in 10-cm
292 plates using calcium phosphate [38]. The medium (8 mL/plate) was replaced 16hrs after
293 transfection. Virus-containing supernatants were harvested 24 h later, filtered through 0.45-
294 µm pore-sized membranes, and stored at -80°C until further transduction. For selection of the
295 resulting polyclonal cell lines, cells were plated at a density of $4.10^4/cm^2$ in a 35 mm Petri dish.
296 The next day later, lentiviral transduction was done using 500 µL of medium to which were
297 added 250 µL of each lentivirus supernatant, for two days. Cells were then put under selective
298 pressure for the expression of both lentiviruses' cassettes using puromycin and blasticidin
299 (Invivogen, gradually increasing concentrations from 4 and 8 µg/mL to 10 and 20 µg/mL within

300 two weeks, comprising two weekly trypsinization procedures). Cell lysates were then
301 generated for netrin-1 KO monitoring by Western blot using the anti-netrin-1 reference
302 Ab126729 (Abcam) prior to liquid nitrogen storage.
303
304 **Netrin-1 release assay**
305 For netrin-1 release assays, Crispr control (HepaRG-Ctrl-KO) and netrin-1 KO (HepaRG-Net-
306 KO#3) cell lines were seeded as depicted above, allowed to reach confluency for 4 days, and
307 sequentially treated with recombinant soluble netrin-1 (125 ng/mL, R&D systems) followed by
308 50 µg/mL poly(I:C) for the indicated times, before supernatant harvesting and its clarification
309 (1,000*g*, 5 min, 4°C). Supernatants were washed with ice-cold PBS and processed for netrin-
310 1 immunoprecipitation and Western blotting.
311

312 **Results**

313

314 Clinical and *in vivo* relevance of netrin-1 induction

315 In order to evaluate the clinical likelihood of an interplay between netrin-1 and inflammation in
316 the liver, we first considered a potential association between netrin-1 and clinical activity
317 scores, performing western blotting (after extensive anti-netrin-1 antibody validation, **see**
318 **Suppl. Fig.1**) on a well characterized HBV-positive series of samples. Samples were selected
319 based on several criteria in order to minimize confounding factors, namely gender (men only
320 here due to availability), similar HBV sample-specific viral loads, fibrosis scores, platelet
321 counts, prothrombin time, ALAT, albumin and bilirubin, leading to a cohort of 14 patients
322 **(Suppl. Table 1)**, the sample sizes of whom were compatible with multitarget immunoblotting.
323 Samples were blotted for netrin-1 and α-SMA, an inflammation-related marker in CLDs [39,
324 40], and association between netrin-1 signals and activity were observed (**Fig.1A**), being
325 however uncorrelated with corresponding netrin-1 mRNA signals **(Fig.1B and Suppl. Fig.3).**
326 Based on activity scores, such data suggest that netrin-1 protein levels are correlated with liver
327 inflammation in HBV patients.

328 In order to probe the robustness of these correlative clinical data, we first investigated the
329 potential impact of experimentally-induced inflammation, using a panel of TLR ligands, namely
330 Pam3-CSK4 as a TLR1/2 agonist, lipopolysaccharide (LPS) as a TLR4 agonist, FLA as a TLR5
331 agonist, FSL as a TLR2/6 agonist, Riboxol (molecularly defined TLR3 agonist), and finally low
332 or high molecular weight poly(I:C) as TLR3, RIG-I and MDA-5 agonists. Experiments were
333 carried out on HepaRG cells as a source of essentially growth-arrested and untransformed
334 cells representative of late-stage CLD [41, 42]. RIG-I was also probed as a control for the
335 induction of inflammation. Pam3CSK4, LPS, FSL, Riboxol, and HMW poly(I:C) induced netrin-
336 1, suggesting its broad spectrum of inflammation triggers, and therefore its relevance, in the
337 hepatic environment (**Fig. 1C**). Chronic viral infections of the liver represent one of the major
338 etiologies of CLDs. Both HBV and HCV viruses have been shown to be direct inducers of
339 dsRNA-based responses [43, 44], which in turn unleash the subsequent inflammation in
340 hepatocytes. HepaRG cells were previously shown to be broadly responsive to poly(I:C) [45].
341 We hereafter focused on the dsRNA analog poly(I:C) of HMW, as a viral mimetic.

342 We then assayed inflammation-related netrin-1 induction in the liver *in vivo*. To achieve this,
343 C57BL/6J mice of both sexes were challenged with HMW-poly(I:C), prior to harvesting their
344 liver, and processing total RNA extracts for RT-qPCR on inflammation-related transcripts.
345 Although poly(I:C) injection did not increase ALT levels (a well-known marker of liver
346 inflammation) in mouse serum within the experimental timeframe (**Suppl Fig.4A**), several
347 other markers of inflammation (*CXCL10*, *IL1B*, *IL6*, *KC*) were induced both in male and female
348 mice. Interestingly, the overall inducibility of canonical inflammation markers was higher in

349 females. (**Suppl. Fig. 4B**). Intriguingly, though *NTN1* mRNA induction was not observed within
350 total RNA populations, a western blot and IHC approach evidenced netrin-1 induction at the
351 protein level, albeit to different extents with female mice being also more responsive (**Fig. 1D-**
352 **E** and **Suppl. Fig. 5**). Such data suggest a causal link between inflammation, inflammation
353 intensity, and netrin-1 induction, at least in the acute inflammatory context. In order to identify
354 the cells implicated in netrin-1 induction, we performed intrahepatic IHC to detect netrin-1 in
355 these murine samples. Netrin-1 staining yielded a homogenous and likely ubiquitous
356 expression pattern, similar to previous data obtained in human liver [9]. Therefore, it is likely
357 that netrin-1 staining was associated with the hepatocytic compartment, which makes up 80%
358 of the liver mass and areas (**Fig. 1F**).
359
360 Translational induction of netrin-1
361 To gain further insight into the mechanisms of netrin-1 production, we conducted a set of *in*
362 *vitro* experiments using HepaRG cells [41] and PHH that present two distinct phenotypes
363 (preneoplastic and fully differentiated, respectively), and are deemed relevant for studying
364 CLD-related mechanisms in untransformed hepatocytic cells. In HepaRG and PHH, poly(I:C)
365 led to netrin-1 protein induction in a dose- and time-dependent manner. The RIG-I inducible
366 marker was monitored to verify poly(I:C) activity. (**Fig. 2A**). As a laminin-related protein [46],
367 netrin-1 is susceptible to be secreted and may also accumulate at the extracellular side of the
368 plasma membrane. We thus tested netrin-1 signals by immunoprecipitation after heparin-
369 based release of plasma membrane-bound netrin-1 in serum-free culture supernatants. Data
370 indicate that the previously observed netrin-1 upregulation by Western blot affects its
371 membrane-bound form along with its presence in the culture medium in both cell types **(Fig.**
372 **2B)**. We then ascertained that its upregulation was independent of its well-documented activity
373 as a cell death inducer. We thus monitored cell viability upon poly(I:C) and heparin treatment,
374 using the neutral red assay in wild-type HepaRG, PHH, and Crispr/Cas9 netrin-1 KO HepaRGs
375 **(Suppl. Fig. 6A-C)**. Previous data were confirmed, indicating that during inflammation, netrin-
376 1 induction is not related to cell injury and is likely involved in cell death-unrelated processes.
377 We next sought to unravel the molecular basis for netrin-1 induction. Similarly to mice, no
378 significant increase in *NTN1* mRNA levels could be evidenced, either in HepaRG cells or in
379 PHH (**Suppl. Fig. 7A**), upon analysis of total RNA pools. Total RNA levels for a given mature
380 transcript depend on various processes that are active in real time, such as transcription,
381 stability, and splicing. We initially focused on pre-mRNA levels, though no significant induction
382 could be observed under poly(I:C) treatment in HepaRG or in PHH (**Suppl. Fig. 7B**). In order
383 to rule out transcriptional induction in such contexts, we then performed a *Ntn1* promoter Luc
384 reporter assay and a run-on assay aiming at quantifying *de novo NTN1* transcription under
385 poly(I:C) treatment. No increase could be obtained following treatment of HepaRG cells with

386 poly(I:C), in either approach, indicating that netrin-1 was not regulated at the transcriptional
387 level (**Suppl. Fig. 8A-B**).
388 To evaluate the possible implication of *NTN1* mRNA splicing in the final phenotype, we
389 calculated the evolution of *NTN1* pre-mRNA over mRNA induction ratios upon poly(I:C)
390 treatment. Again, no significant alteration of such ratios was observed (**Suppl. Fig. 9**),
391 suggesting that regulation of splicing did not participate in netrin-1 protein increase. In order to
392 safely orient subsequent studies towards post-transcriptional read-outs, we lastly quantified
393 *NTN1* mRNA stability using the selective RNA polymerase II inhibitor triptolide [47]. In this
394 assay, *NTN1* mRNA decay rate was unaltered (-1.3-fold) by poly(I:C) (**Suppl. Fig. 10**), arguing
395 in favor of a post-transcriptional regulation.
396 Following the next step in the biogenetic processing of netrin-1, we then considered
397 translational regulation as a potential contributor to netrin-1 protein induction. We first
398 submitted HepaRGs, PHHs and mouse livers to total polysomal fractionation using sucrose
399 gradient-based isopycnic ultracentrifugation followed by gradient trace monitoring, RNA
400 extraction, and RT-qPCR on the *NTN1* transcript. Adequate fractionation could be evidenced
401 using gradient UV traces. The presence of the peak of free messenger ribonucleoparticles
402 (mRNPs), followed by the 40S, 60S and 80S ribosomal subunits, themselves finally followed
403 by the typical oscillating profile of successive polyribosomes was delineated (**Fig. 3A,** black
404 and red traces). As expected, translation was more active in early confluent HepaRG cells (as
405 previously depicted [48]) than in resting, optimally differentiated, PHH, or mouse livers.
406 Moreover, for HepaRG cells, the percentage of polysome-bound *NTN1* mRNA signals versus
407 total *NTN1* signals remained unchanged upon poly(I:C) treatment (87.9% versus 86.0% in
408 treated cells), whereas in PHH, a major shift of the *NTN1* signal could be observed towards
409 the polysomal compartment of the gradient (46% versus 89%, $p < 0.05$) **(Fig. 3B-C)**. The
410 absence of changes in mouse livers is concomitant to higher amounts of *NTN1* in heavy
411 polysomes (fractions 13-17), that are associated with strong translational activity. In order to
412 confirm this, an EDTA release control experiment was carried out. EDTA induces polysomal
413 collapse through Mg^{2+} and Ca^{2+} chelation, enabling the evaluation of the genuine polysomal
414 origin of the RT-qPCR signals, and reinforced these results (**Fig. 3A-C**).
415 Altogether, our data advocate for distinct modes of regulation of netrin-1 induction in HepaRG
416 hepatocyte-like cells and fully differentiated environments such as PHH and mice livers. Mouse
417 livers and PHH appear to activate total polysome-based translation of the *NTN1* transcript for
418 the final induction of the protein. Yet, netrin-1 biogenesis mechanisms remain uncharted at
419 this stage of the study in HepaRG cells, which are representative of late stage, preneoplastic,
420 CLD.
421 In order to pursue the identification of the molecular basis of netrin-1 increase upon poly(I:C)
422 treatment in HepaRG cells, the *de novo* incorporation of labeled amino acids into the netrin-1

423 sequence was quantified by MS after netrin-1 immunoprecipitation, using stable isotope
424 labeling by amino acids in cell culture (SILAC) method. This SILAC approach indicated a 4.5-
425 fold increase in *de novo* incorporation of amino acids in inflammatory conditions versus naïve
426 cells (**Fig.3D-E**). These data suggest that if translation *per se* is not modulated in HepaRG
427 cells, as found by polysomal fractionation, processes increasing the susceptibility of the *NTN1*
428 transcript to translation are strong candidates.
429
430 Staufen-1 mediates netrin-1 induction through direct interactions with the *NTN1* transcript in
431 preneoplastic cells
432 A majority of the transcriptome encoding secretory and membrane proteins is ER-bound [49].
433 Netrin-1 is a secreted protein and its translation should naturally take place in association with
434 the endoplasmic reticulum (ER) membranes so that co-translational translocation of the
435 nascent peptide across the ER membrane may occur through the transient association of the
436 peptide's signal sequence with the translocon [50]. Therefore, netrin-1 translation is
437 conditioned by two distinct events: association with polyribosomes and accumulation of the
438 transcript at the ER level for subsequent transfer of the native peptide to the secretory pathway.
439 We took into consideration this process in order to determine divergences between HepaRG
440 cells and PHH for netrin-1 induction. Based on the so-called 'sequential extraction' method
441 [32, 33], which allows the investigation of mRNA partitioning between cytosol and microsomes,
442 we verified netrin-1 enrichment following poly(I:C) treatment using three protein markers (RIG-
443 I and caspase-3 as cytosolic proteins and the ER-associated PDI/P4HD protein, **Fig. 4A**).
444 Whereas no significant alteration in cytosolic or membrane-bound levels of *NTN1* transcripts
445 was evidenced upon poly(I:C) treatment in PHH, the level of *NTN1* transcript enrichment in
446 membrane-bound versus cytosolic fractions increased by 7-fold in inflammatory HepaRG cells
447 ($p < 0.05$; **Fig. 4B)**. These finding indicate that translational induction of netrin-1 occurs via the
448 transfer of the *NTN1* transcript to the ER prior to its active translation in HepaRG cells.
449 We then focused on *NTN1* mRNA relocalization by conducting a bibliographic search for
450 proteins participating in transport and translational regulation of highly structured, GC-rich,
451 mRNAs in their 5' ends, which the *NTN1* transcript belongs to [16]. The double-stranded RNA
452 binding domain-containing protein Staufen-1 (STAU1) shuttles between the cytosol and the
453 ER thanks to its association with microtubules through its tubulin binding domain [51, 52].
454 STAU1 is implicated in translational activation of GC-rich, structured, mRNAs 5'UTRs [53], and
455 was shown to bind to the *NTN1* transcript in high throughput experiments [54, 55].
456 In resting cells, STAU1 displayed a granular staining also observed in other studies, where it
457 associates with RNA granules before or after movement on microtubules [56-59]. Interestingly,
458 poly(I:C) triggered the reconfiguration of STAU1 signals from a granular to a microtubule-like
459 filamentous pattern, in accordance with other studies [51, 52, 56]. The number of STAU1-

460 positive granular foci per cell decreased 11-fold and the percentage of STAU1 filamentous
461 staining-positive cells increased 9-fold with poly(I:C) (**Fig.5A-B**). STAU1 staining also
462 displayed an increased overlap with PDI+ (ER) areas, quantified using the Li colocalization
463 coefficient. (**Fig. 5C-D**)
464 In order to test direct interactions between Staufen-1 and the full length netrin-1 mRNA in our
465 biological setting, we set-up a CLIP assay in UV cross-linked HepaRG cells using a variety of
466 relevant negative and positive control transcripts [54, 55]. Immunoprecipitation conditions for
467 STAU1 were first defined (**Fig. 6A**). Data depicted in this panel show significant increase in
468 *NTN1* levels versus several other transcripts, in addition to a specific and positive impact of
469 poly(I:C) *per se* on *NTN1* binding levels to STAU1. Percentages of transcript inputs are
470 indicated in poly(I:C)-treated or untreated conditions in **Fig. 6B**.
471 To further probe such interactions, we carried out a filter binding assay, which provides
472 information on the affinity of both partners and their class of interaction dynamics downstream
473 of collected STAU1-bound, RNA-conjugated, biotin-avidin-HRP signals. Based on obtained
474 profiles, filter binding data were fit to a sigmoidal equation to determine binding constants and
475 to estimate the degree of binding cooperativity. Calculation of Kd led to a value of 1.17+/-0.11
476 nM. Calculation of the Hill constant was done using the previously published formula: Log (81)
477 / Log (EC_{50}/EC_{10}) [60] and led to a value of 1.9+/-0.28, suggesting a moderately cooperative
478 interaction. As a control, no interaction between an HBV epsilon loop RNA sequence and
479 STAU1 was observed. In competition experiments, incubation of increasing concentrations of
480 unlabeled *NTN1* 5'UTR led to displacement of the pre-bound labeled RNA as expected, while,
481 again, no reversion of STAU1-NTN1 5'UTR complex-derived signals could be achieved using
482 HBV control RNA **Fig.6C-D.** Altogether, such data suggest that the dsRNA binding protein
483 STAU1 directly binds to the 5'UTR of the netrin-1 transcript, corroborating the accumulation of
484 STAU1 at the ER level for enhanced susceptibility of this secreted protein's mRNA to
485 translation upon poly(I:C) treatment.
486 In order to unequivocally test the functional implication of STAU1 in the accumulation of the
487 *NTN1* transcript at ER sites for netrin-1 protein induction, we tested the effect of RNAi-
488 mediated STAU1 depletion on poly(I:C)-induced *NTN1* accumulation at the ER and on netrin-
489 1 induction. Both approaches showed reversion of poly(I:C)-induced netrin-1 signals **(Fig. 6E-**
490 **G)**. Moreover, these mechanistic data indicated that Staufen-1-dependent transcript transfer
491 to the ER in non-differentiated cells (here represented by proliferative HepaRG cells),
492 determined netrin-1 induction *in vitro*. They represent to our knowledge the first functional
493 description of Staufen-1 in inflammation. A comparison of results obtained in HepaRG cells
494 and PHH suggests that mRNA relocalization and translational activation seem to be mutually
495 exclusive mechanisms across both cell environments, yet converging and enabling netrin-1
496 induction.

497

498 Netrin-1 induction is unrelated to post-translational steps

499 In order to potentially define RNA relocalization as a unique contributor to netrin-1 upregulation
500 during inflammation, the susceptibility of netrin-1 to enhanced secretion as well as its stability
501 were considered downstream of this experiment. The hepatocyte is one of the major secretory
502 cells of the human body. Since inflammation is also potentially regulated at the secretion level
503 because of its important cytokinic component, we considered a potential impact of poly(I:C)
504 treatment on cell secretion, which could itself regulate netrin-1 levels downstream of
505 translation. Using the so-called RUSH (retention using selective hooks) assay [36] we treated
506 or not HepaRG cells with poly(I:C) and, using immunofluorescence, we examined the ability of
507 a fluorescent fusion form of alpha1-antitrypsin (AAT-GFP) to reach the Golgi apparatus
508 (located using giantin staining) within the assay timeframe. As shown in **Suppl. Fig. 11A-B**,
509 no noticeable difference was observed between colocalized signals derived from GFP or
510 giantin in treated versus untreated cells. AAT being one of the most abundant and specific
511 cargoes of the hepatocyte, such data suggest that the global secretory activity levels of
512 HepaRG cells are not altered by poly(I:C), and that netrin-1 levels remain unaffected by this
513 regulatory step.

514 To rule out the accumulation of netrin-1 through protein stability enhancement, we stopped
515 translation by cycloheximide treatment prior to harvesting poly(I:C)-treated HepaRGs and PHH
516 in a time-course assay and combined immunoprecipitation of cell-bound and secreted netrin-
517 1. In these conditions, no alteration of netrin-1 protein decay rate could be evidenced (**Suppl.
518 Fig. 12**). In association with previous data, these two last datasets provide final evidence that
519 netrin-1 induction occurs through transcript localization regulation (undifferentiated HepaRGs)
520 and translational activation (PHHs).

521

522 Induction mechanistics are constrained by the pathogenic status of origin of the cells

523 While HepaRG cells are capable of undergoing partial experimental hepatocytic re-
524 differentiation under defined culture conditions, their pre-neoplastic status is established by
525 their peritumoral origin in a cirrhotic liver [41]. In order to control netrin-1 induction mechanisms
526 between HepaRG and PHH for the former's pathological origin, we submitted HepaRG cells
527 to their usual hepatocytic differentiation protocol [42]. In polarized, quiescent and differentiated
528 HepaRG, of note again, no *NTN1* induction occurred at the total RNA level in a context where
529 netrin-1 protein is induced by poly(I:C). Yet, netrin-1 protein induction correlated with
530 accumulation of *NTN1* mRNA in the membrane-bound compartment (**Suppl. Fig. 13**), as was
531 the case with undifferentiated HepaRGs. This dataset indicates that the nature of post-
532 transcriptional processes converging to netrin-1 induction is more constrained by the

533 pathological status of origin of the cells with respect to pre-neoplastic (HepaRG) or
534 physiological (PHH) hepatic contexts than by their level of differentiation
535
536 A phase 2 trial-validated antibody enabling netrin-1 capture dampens inflammation in mice
537 As published in several studies, tissular inflammation may be altered by netrin-1 [20-22, 61]
538 suggesting its mobilization in interstitial fluids. To test whether netrin-1 may act as an
539 auto/paracrine factor with diffusible consequences, we monitored the behavior of exogenously
540 added in-house validated recombinant netrin-1 [9], on netrin-1 KO Crispr cells upon poly(I:C)
541 treatment. Using netrin-1 immunoprecipitation and Western blot, we observed that poly(I:C)
542 mobilized netrin-1 within 2 hours from its cell-associated pool towards supernatants (**Suppl.**
543 **Fig. 14)**, hence arguing in favor of its regulatory role in hepatic inflammation at the
544 microenvironmental level.
545 Considering that this diffusible status corroborated previously known tissular effects of netrin-
546 1 [20-22, 61], we treated C57BL/6J mice with the clinically used and well tolerated anti-netrin-
547 1 antibody NP137 (NCT02977195) [27] or its NP001 isotypic control 32h before challenging
548 them with poly(I:C) for 16h and liver harvest. Treatment with the former did dampen poly(I:C)-
549 induced netrin-1 induction (**Fig.7A**), that occurred, again, independently of *NTN1* RNA
550 upregulation in all instances (**Fig.7B**). RT-qPCR conducted on a panel of inflammation-related
551 cytokines (*CCL2, CXCL10, IL1B, IL6, KC* (ortholog of human IL8), *IL12B, IL15,* and *TGFB1*
552 highlighted a causal relationship between netrin-1 inactivation and reversion of the induction
553 of several of these cytokines (*CCL2, CXCL10, IL1B, KC*, and *TGFB1,* **Fig. 7B**). In order to
554 further document this phenotype, we performed a flow cytometry analysis to monitor immune
555 cell population regulation. Gating strategies are shown in **Suppl. Fig.15**, where the three left
556 panels depict Ly6C^{+} CD11^{low} F4/80^{hi} gating (from top to bottom: Poly(I:C)+ and NP001,
557 Poly(I:C)+ and NP137, and finally Ly6C FMO on pooled cells from all mice). Monocyte-derived
558 macrophages (CD45^{+} CD11b^{+} F4/80^{low}) remained stable. Total Kupffer cells (CD45^{+} CD11b^{low}
559 F4/80^{hi}) counts were not regulated. However, the NP137 antibody reversed Ly6C^{+} Kupffer cells
560 counts. (**Fig.7C**). Hence, such data suggest that netrin-1 is an actionable target that further
561 amplifies dsRNA-triggered liver inflammation, in accordance with its role in other organs 1 [20-
562 22].
563

564 **Discussion**

565

566 Netrin-1 has been repeatedly identified as a cancer promoting agent [5, 6, 10-15]. Its
567 expression is associated with inflammatory diseases that may themselves promote cancer
568 onset [6, 26]. Given the causal link between inflammation, cirrhosis, and HCC [62-66], probing
569 the direct impact of inflammation on netrin-1 expression in the liver was of interest.
570 Although transcriptional regulation has been considered a hallmark regulatory step in general
571 cell biology and liver differentiation processes [67], increasing evidence suggests that
572 processes that need swift temporal regulation in highly remodeled tissues, such as
573 inflammation and, more generally, oncogenic processes and associated resistance, rely on
574 translational modulation [68, 69].
575 Our experience in the liver field has been recurrently confronted with this type of regulation.
576 Indeed, differentiation of HepaRG cells is strongly associated with important downregulation
577 of a majority of transcripts at the total RNA level, together with a concomitant upregulation in
578 polysomal fractions of a subset of hepatocytic differentiation-related mRNAs [70].
579 Experimental activation of the mTOR/S6 kinase pathway, which is present in 45% of HCC
580 cases [71], impairs hepatocytic differentiation, and impedes the translation of transcripts
581 moderating lipid homeostasis and cell growth [31]. Upon the UPR, netrin-1 translation is
582 selectively favored during global translational shut down, together with IRES-bearing
583 transcripts implicated in cell survival and transformation [72]. Finally, the netrin-1 receptor
584 UNC5-A is also translationally down-regulated upon HCV infection, including in patient livers
585 [8]. Moreover, the liver is one, if not the most, active secretory and metabolic cell type in human
586 physiology, in line with being exposed to real-time needs for metabolic and hence secretory
587 regulation (acute phase, post-prandial phases). It is thus conceivable that the biogenesis of
588 secreted factors such as netrin-1 are more often constrained by swift regulatory processes
589 such as translational control in the liver than in other cell types. The present data, to be
590 interpreted as a confirmation of the particular susceptibility of netrin-1 to post-transcriptional
591 regulation, strengthens the need for more frequent molecular analyses of pathogenic
592 processes using total RNA-unrelated enrichment methods, such as polysomal profiling, at least
593 at the liver level.
594 In the present study, we have shown, depending on the cell system of interest, *i.e.*
595 undifferentiated HepaRG or PHH, that netrin-1 biogenesis under inflammation was specifically
596 regulated at the mRNA localization level in the former, while at the translational level *per se* in
597 the latter case and that the pathogenic status of the cells conditioned these modes of induction.
598 The presence of these mechanisms is of interest, since it appears that two distinct modes of
599 post-transcriptional regulation actually converge towards a single phenotypic outcome, i.e.,
600 netrin-1 increase. Pathophysiological needs for delivering this final phenotype therefore seems

601 to override cell type-specific functional singularities, suggesting that induced netrin-1 conveys
602 important functions in the liver, either immunomodulatory [20-22, 61], or, on the long-term,
603 hepatoprotective as an anti-apoptotic factor [5, 6, 10-15].
604 This phenotype relies on the RNA-binding protein Staufen-1, the implication of which is to date
605 essentially undocumented in the regulation of inflammatory processes. However, Staufen-1
606 has recently been shown to foster gastric cancer progression in a cyclin-dependent kinase-
607 dependent manner [73] and also to take part in an EZH2-related, HCC promoting pathway
608 [74], suggesting relevance of further studies aiming at characterizing its implication in end-
609 stage liver disease through a possible netrin-1 involving axis.
610 From a more pathology- and therapy-oriented point of view, this study suggests a potential link
611 between hepatic inflammation and liver disease progression through netrin-1. To date, in the
612 liver, direct cross-talks between inflammation and HCC have been mainly defined through the
613 IL-6/gp130/STAT3 axis [75]. We previously documented that progression towards HCC is
614 associated with a sharp drop in *UNC5A* (netrin-1 receptors) expression levels [8], thereby
615 functionally augmenting netrin-1 activity, following the dependence receptor theory [76]. Our
616 study improves the understanding of the potential implication of inflammation in the evolution
617 of CLDs, besides the well characterized IL-6/gp130/STAT3 cascade and identifies an
618 actionable target for its modulation. Chronic inflammation of a given tissue is counterbalanced
619 by a wound healing process leading to scar, acellular, tissue build up, made of ECM. As
620 mentioned before, netrin-1 is a laminin-related protein that shares several structural features
621 with ECM-constituting proteins. As a consequence, one may hypothesize that netrin-1 could
622 participate in ECM build-up. The fact that netrin-1 promotes fibrosis in the inflammatory lung
623 [77] strengthens the potential relevance of this hypothesis.
624 The humanized anti-netrin capture antibody NP137 developed by the authors [27] is currently
625 under investigation in phase 2 clinical trials in general oncology (US Clinical Trials #02977195)
626 and shows no clinical toxicity in a diversity of solid tumors contexts. The apparent anti-
627 inflammatory activity of this antibody in the present setting argues in favor of its eventual
628 transfer to the clinic for subsequent trials in histologically evolutive CLDs.
629

630 **Acknowledgements**

631 We thank B Bancel (pathologist, Lyon U. Hospital) for determining the activity scores, L Muller
632 for technical assistance, A Paradisi for the netrin-1 promoter reporter plasmid, the CIQLE
633 platform for assistance with confocal microscopy, and B. Manship for editing. RB and IC are
634 recipients of a DevWeCan Labex (Laboratories of Excellence Network, ANR-LABX-061) and
635 ANRS (ECTZ63958) predoctoral fellowships, respectively. Funding has been obtained through
636 the same Labex consortium (ANR-LABX-061) and the French NCI (Inca PRT-K 19-033).
637 Proteomic experiments were partially supported by the French NRA under projects ProFI

(Proteomics French Infrastructure, ANR-10-INBS-08) and GRAL, a program from the Chemistry Biology Health (CBH) Graduate School of University Grenoble Alpes (ANR-17-EURE-0003).

641 **Figure legends**

642

643 **Figure 1**

644 **Netrin-1 levels are correlated with activity scores in HBV-positive clinical liver**
645 **specimens, induced in HepaRG cells by several TLR ligands and induced by poly(I:C)**
646 **in mouse livers.**

647 **A**. HBV-infected liver tissues (clinico-biological features listed in supplementary table 1) were
648 homogenized using a Dounce homogenizer in lysis buffer, centrifuged to remove debris,
649 denatured, and visualized by SDS-PAGE. Netrin-1 and α-SMA were probed using antibodies
650 listed in **Suppl. Table 2**. Since actin staining is not correlated with the amount loaded, Ponceau
651 staining is shown as well. **B**. Corresponding RNA data are plotted versus activity scores. **C**.
652 Netrin-1 expression levels were evaluated by immunoblotting (n = 3 independent experiments).
653 RIG-I was used as a poly(I:C) activity control. **D**. The levels of *NTN1* mRNA were quantified
654 by RT-qPCR using *GUS* [78] as an internal reference. Mann-Whitney test (n.s.). **E**. Netrin-1
655 expression levels were evaluated by immunoblotting using anti-RIG-I and anti-netrin-1
656 antibodies. **F**. Liver slides were probed with the same anti-netrin-1 antibody prior to secondary
657 antibody incubation and HRP-based visualization. Mouse samples were derived from the same
658 hepatic lobe in all instances. Data are representative of a total of 40 mice (10 females, 10
659 males, +/- poly(I:C); **see Suppl. Fig. 4** for comprehensive data).

660

661 **Figure 2.**

662 **Cell-associated and soluble netrin-1 levels are upregulated by poly(I:C) in a time- and**
663 **dose-dependent manner in HepaRG cells and in PHH.**

664 **A**. Netrin-1 expression levels were evaluated by immunoblotting using an anti-netrin-1 antibody
665 (n = 3, HepaRG; and n = 3 distinct PHH batches). RIG-I was used as a poly(I:C) activity control.
666 **B**. Netrin-1 expression levels were evaluated by immunoblotting in total cell lysates or after
667 immunoprecipitation in supernatants, with or without heparin. NP001: isotype control. NP137:
668 anti-netrin-1 Ig. RIG-I was used as a poly(I:C) activity control.

669

670 **Figure 3.**

671 **Inflammation activates translation of the *NTN1* transcript in HepaRG cells, PHH and**
672 **mouse livers.**

673 HepaRGs, PHH and mouse livers samples were homogenized in polysome lysis buffer and
674 loaded onto a linear sucrose gradient prior to isopycnic ultracentrifugation. **A**. Representative
675 profile of UV gradient traces. **B**. *NTN1* distribution profile across the gradient. Total
676 polyribosomes were fractionated, extracted and processed for *NTN1* by RT-qPCR (n = 3,
677 HepaRG; n = 3 distinct PHH donors, n = 6 female mice). Mann–Whitney test, * $p < 0.05$. **A-B**.

678 An EDTA release control assay was performed by adding EDTA to lysates immediately before
679 ultracentrifugation (green values). **C.** Quantification of corresponding polysomal signals. **D.**
680 Total lysates and supernatants derived from treated and control HepaRG cells previously
681 adapted to dialyzed serum conditions for 14 days (and labeled with medium or heavy Lys or
682 Arg isotopes supplemented in Lys/Arg-free William's E medium) were lysed with 5x lysis buffer
683 and quantified for total protein amounts and mixed 1:1 prior to netrin-1 immunoprecipitation.
684 **E.** Immunoprecipitated material was then run onto SDS-PAGE, submitted to tryptic digestion
685 and subsequent isotope-specific mass spectrometry-based quantification (n = 3 independent
686 experiments). The schematic diagram was drawn using the BioRender software. Mann-
687 Whitney test, *** $p < 0.001$.
688
689 **Figure 4**
690 ***NTN1* accumulates in membrane/ER-positive fractions upon poly(I:C) treatment in**
691 **HepaRG cells.**
692 The Stephens et al. sequential extraction method was used as mentioned in the materials and
693 methods section. **A**. Adequate partitioning was verified by Western blotting on PDI (internal
694 membrane contents) and caspase-3 (cytosolic contents). RIG-I (cytosolic location) was also
695 probed as a poly(I:C) activity control. Differential Ponceau Red staining profiles are shown. **B**.
696 *NTN1* transcripts were monitored for their partitioning by RT-qPCR. Mann-Whitney test, * $p <$
697 0.05 (n = 3 (HepaRG), and n = 3 distinct PHH batches).
698
699 **Figure 5**
700 **Poly(I:C) induces Staufen-1 relocalization and accumulation at endoplasmic reticulum,**
701 **PDI-positive, sites.**
702 **A.** Representative immunofluorescence-based localization of PDI (red) and Staufen-1 (green).
703 Nuclei were counterstained with Hoechst 33342. **B.** Number of Stau1-positive dots per cell and
704 percentage of fibrillar Stau1-positive cells versus total cells are shown under resting or
705 poly(I:C)-treated conditions. Mann-Whitney test after Shapiro-Wilk test (* $p < 0.05$, n = 3
706 independent experiments). **C.** Li diagrams and Li coefficient calculations for PDI and Staufen-
707 1 colocalization quantification, respectively. Pixels present on the left and right sides of the y-
708 axis, i.e., associated with negative and positive staining amplitude values, indicate exclusion
709 and colocalization, respectively. Li coefficients were calculated using the JACop plugin from
710 the ImageJ software (http://rsb.info.nih.gov/ij/plugins/track/jacop.html). Twenty random fields
711 were acquired per biological sample, totaling 300-400 cells analyzed for each biological
712 sample in a given single experiment (n = 3 independent experiments). **D.** Statistical
713 assessment of the colocalization of PDI and Staufen-1. Red (PDI) and green (Stau1)
714 fluorescence intensities were measured for each pixel along a 5µm line, using the Plot Profile

715 function of the ImageJ software. Spearman correlation coefficients for each couple of intensity
716 values are indicated.
717
718 **Figure 6**
719 **Staufen-1 interacts with *NTN1* mRNA through its 5'UTR, and conditions *NTN1* transcript**
720 **relocalization and netrin-1 induction in proliferative HepaRG**
721 **A.** CLIP / Staufen-1 immunoprecipitation. HepaRG cell lysates derived from UV crosslinked
722 monolayers were immunoprecipitated with naked, IgG control or anti-STAU1-coupled beads
723 prior to elution and 1D SDS-PAGE. **B.** negative control (mitochondrial) transcripts, positive
724 control [54] transcripts for STAU1 binding, and *NTN1* were quantified on immunoprecipitated
725 materials relatively to inputs. Mann-Whitney test, *** $p < 0.01$ (n = 5 independent experiments).
726 **C.** Filter binding assay. Biotin-labeled *NTN1* 5'UTR or HBV RNA epsilon loop at constant
727 amounts were titrated for their ability to undergo trapping by the upper nitrocellulose membrane
728 ('Nitro') or reach the lower nylon membrane ('N+') by increasing amounts of recombinant
729 STAU1 protein. Corresponding quantification of HRP signals and obtained parameters are
730 shown. **D**. Competition experiments using the filter assay approach. Pre-bound STAU1-*NTN1*
731 5'UTR biotin(+) complexes were submitted to increased concentrations of unlabeled
732 competitors (*NTN1* 5'UTR or HBV epsilon RNAs) and processed on both membranes.
733 Corresponding quantification of HRP signals and obtained parameters derived from one
734 representative experiment because of variability are shown (n = 5 independent experiments).
735 **E**. Impact of Staufen-1 depletion on netrin-1 induction was evaluated by immunoblotting. **F**.
736 Adequate partitioning between cytosolic (C) and membrane (M) fractions was addressed by
737 Western blotting on PDI (internal membrane contents) and caspase-3 (cytosolic contents).
738 RIG-I (cytosolic location) was probed as a poly(I:C) activity and cytosolic control. **G**. *NTN1* was
739 then quantified by RT-qPCR in both fractions. Mann-Whitney test, **$p < 0.01$ (n = 3
740 independent experiments).
741
742 **Figure 7**
743 **Netrin-1 capture by a clinically used antibody dampens hepatic inflammation in mice.**
744 **A**. Hepatic netrin-1 levels were measured by western blotting. **B**. *NTN1* and indicated cytokines
745 mRNAs levels were quantified by RT-qPCR using the *GUS* transcript as a reference. **C**.
746 Percentage of positive live (DsRed) cells against CD45, CD11b, F4/80, Ly6C, CD3, CD8 and
747 CD69 markers are indicated in the presence or absence of poly(I:C) and netrin-1 inactivation
748 (n = 5-8 mice per group).
749
750 **Figure 8**

751 **Netrin-1 is a pro-inflammatory factor up-regulated upon inflammation by exclusive**
752 **translational activation or Staufen-1 dependent regulation processes in the liver.**
753 Poly(I:C) drives netrin-1 upregulation in hepatocytes through translational activation or
754 Staufen-1-mediated accumulation to the ER membrane. Poly(I:C) alters netrin-1 binding to the
755 extracellular side of the membrane and potentiates its activity as a secreted soluble factor.
756 Blocking netrin-1 signaling with NP137 reverses Kupffer cells activation and pro-inflammatory
757 cytokine transcripts amounts in total liver extracts.
758
759 **Supplementary Figure 1.**
760 **In-house assessment of anti-netrin-1 antibody staining reliability.**
761 **A-B**. A panel of hepatocyte-like cell lysates derived from *NTN1* mRNA negative or positive
762 cells was probed by RT-qPCR and netrin-1 Western blotting, respectively, using the Abcam
763 reference Ab126729. **C-D**. Crispr/Cas-9 engineered netrin-1 KO HepaRG cells and *NTN1*
764 siRNA-treated HEK293T cells, respectively, were subjected to anti-netrin-1 immunoblotting
765 using the same antibody.
766
767 **Supplementary Figure 2.**
768 **Sequential extraction method.**
769 Phase contrast microscopy of sequential extraction steps are shown for HepaRG cells. **A.** After
770 stripping the intact cells of their cytoplasm (left panel) and then of their internal membrane
771 contents (center), only nuclei remain visible as attached to the plastic dish (right panel, **B**).
772
773 **Supplementary Figure 3.**
774 **Netrin-1 protein levels and transcripts are not correlated in human liver tissues.**
775 HBV-infected liver tissues (clinico-biological features listed in supplementary table 1) RNA data
776 are stratified in a sample specific manner.
777
778 **Supplementary Figure 4.**
779 **Poly(I:C) activity assessment in mice.**
780 **A**. ALT activity was monitored in the serum of the same mice challenged with poly(I:C). n = 10
781 females and 10 males, +/- poly(I:C), corresponding to 40 animals. * $p < 0.05$, ** $p < 0.01$, Mann-
782 Whitney test after Shapiro-Wilk test. ULN, upper limit of normal values. **B**. C57BL/6J mice were
783 challenged with poly(I:C), their liver harvested, and total RNA extraction processed for RT-
784 qPCR on inflammation-related transcripts. Corresponding canonical markers of inflammation
785 activation (*IL1B*, *IL6*, *CXCL10, KC* (ortholog of h*IL8*)) were monitored.
786
787 **Supplementary Figure 5.**

788 **Dot blot quantification of netrin-1 using in-house validated anti-netrin-1 antibody**.
789 **A.** Ponceau staining was used as a loading reference. N = 10 females and 10 males, +/-
790 poly(I:C), corresponding to 40 animals.
791
792 **Supplementary Figure 6.**
793 **Poly(I:C) does not alter cell viability in HepaRG and PHH.**
794 Viability was quantified by the Neutral Red assay. **A.** n = 3 (HepaRG); n = 3 distinct PHH
795 batches, **B.** n = 3 (Netrin-1-KO and control Crispr/Cas-9 HepaRG). Mann-Whitney test (n.s.).
796 **C**. Cells were treated with heparin overnight prior to harvesting (HepaRG, n = 3, n.s).
797
798 **Supplementary Figure 7.**
799 ***NTN1* total RNA and pmRNA levels are unaffected by poly(I:C) either in a time- or dose-**
800 **dependent manner in HepaRG cells and in PHH.**
801 **A**. The levels of *NTN1* mRNA were quantified by RT-qPCR using *GUS* as an internal reference.
802 Statistical significance was determined using the Mann-Whitney test. (n.s.). **B.** The levels of
803 *NTN1* pre-mRNAs (intron 1) were quantified likewise. No amplification occurred when using
804 heat-inactivated RT (green square). Mann-Whitney test (n.s.). n = 3 independent experiments
805 (HepaRG); n = 3 distinct PHH donors run in technical triplicates.
806
807 **Supplementary Figure 8.**
808 ***NTN1* transcription is not induced by poly(I:C) in HepaRG cells.**
809 **A**. The levels of *Ntn1* promoter-dependent Luciferase expression were evaluated using a *Ntn1*
810 promoter (-1740; +1) Luc expressing plasmid. **B**. Quantification of *de novo* transcription of
811 *NTN1* using a run-on assay. Mann-Whitney test (* $p < 0.05$).
812
813 **Supplementary Figure 9**
814 ***NTN1* mRNA splicing remains unaffected by poly(I:C).**
815 **A**. *NTN1* mRNA over pmRNA ratios were calculated. Mann-Whitney test (n.s.). n = 3
816 independent experiments (HepaRG), and n = 3 distinct PHH batches run in technical
817 triplicates.
818
819 **Supplementary Figure 10**
820 ***NTN1* transcript stability is not regulated by poly(I:C).**
821 HepaRG cells were treated with poly(I:C) for 48hrs before adding the RNA polymerase II
822 inhibitor triptolide to the medium and harvesting cells at different time points to quantify *NTN1*
823 and *c-fos (FOS)* by RT-qPCR. **A.** Total mRNA integrity throughout the experimental time-
824 course was monitored using the Bioanalyzer device. **B.** *c-fos* levels collapse was used as a

825 control for assessing triptolide activity. **C.** *NTN1* transcript decay rate in control and poly(I:C)-
826 treated conditions was calculated. n = 3 independent experiments. Mann-Whitney test (n.s.).
827
828 **Supplementary Figure 11**
829 **Poly(I:C) does not alter the functionality of the hepatocytic secretory pathway using**
830 **A_1AT as a hepatocyte-specific major cargo.**
831 **A.** HepaRG cells were transfected with A_1AT-GFP bearing plasmids in biotin-free medium and
832 treated or not with poly(I:C). **B.** GFP and giantin colocalization were then estimated in a time
833 course assay after the addition of biotin to the medium (means of n = 2 independent
834 experiments are shown). Mann-Whitney test (n.s.).
835
836 **Supplementary Figure 12**
837 **Netrin-1 protein stability is not modified by poly(I:C)**
838 Cells were treated by poly(I:C) for 48 hours and with cycloheximide at 48 hours to stop
839 translation. **A.** Cells and supernatants were then harvested and total netrin-1 pools
840 immunoprecipitated before immunoblotting with netrin-1 antibody. **B.** Densitometry was
841 performed to evaluate protein amounts (n = 6 independent experiments).
842
843 **Supplementary Figure 13**
844 **Netrin-1 induction in differentiated HepaRG cells relies on relocalization of the *NTN1***
845 **transcript.**
846 **A**. Netrin-1 expression levels were evaluated by immunoblotting using an anti-netrin-1
847 antibody. Inflammation induction was verified using anti-RIG-I antibody. **B**. *NTN1* expression
848 levels were quantified by RT-qPCR. Mann-Whitney test (n.s.). **C**. Differentiated HepaRG were
849 treated with cycloheximide, scraped, lysed and loaded atop of a linear sucrose gradient prior
850 to isopycnic ultracentrifugation. Representative profile of UV gradient traces is shown. **D**. *NTN1*
851 distribution profile across the gradient was identified by RT-qPCR. **C-D.** An EDTA release
852 control assay was performed by adding EDTA to lysates immediately before ultracentrifugation
853 (green values). **E**. Percentages of polysomal *NTN1* transcripts versus total are shown (n = 3).
854 Mann-Whitney test (n.s.). **F**. Adequate partitioning was addressed by western blotting on PDI
855 (internal membrane contents) and caspase-3 (cytosolic contents). RIG-I (cytosolic location)
856 was probed as a poly(I:C) activity control. **G**. *NTN1* transcripts were monitored for their
857 partitioning by RT-qPCR. Mann-Whitney test, * $p < 0.05$. (All data shown derive from n = 3
858 independent experiments).
859
860 **Supplementary Figure 14**
861 **Inflammation mobilizes netrin-1 from its cell-associated pool.**

862 Netrin-1 KO Crispr/Cas9 HepaRG cells were pretreated with recombinant netrin-1 (previously
863 in-house validated for activity [9]) for 4 hours, and subsequently incubated with poly(I:C). for
864 the indicated times. Cells were then submitted to total lysates- and IP-based immunoblotting
865 for RIG-I as a poly(I:C) activity control and netrin-1. Tubulin and Ponceau staining were
866 performed to ascertain purity of extracellular IP material. One experiment out of three is shown.
867
868 **Supplementary Figure 15**
869 **Gating strategy for FACS experiment on mouse livers.**
870 Live cells singlets of interest were gated prior to CD45+ sorting. Monocyte-derived
871 macrophages are $CD45^{+}$ $CD11b^{+}$ $Ly6G^{-}$ $F4/80^{lo}$. Kupffer cells are $CD45^{+}$ $CD11b^{lo}$ $Ly6G^{-}$
872 $F4/80^{hi}$, and $Ly6C^{+}$ when pro-inflammatory.
873

874 **Suppl. Table 1. Clinico-biological features of clinical samples**

875 **A.**

	median (range)
N	14
Sex	men
age	68 (41 -83)
etiology	HBV
HBV RNA (copy / mL)	2,281,132 (1,958 - 1,215,827,224)
Metavir activity (A0)	3
Metavir activity (A1)	9
Metavir activity (A2)	2
Metavir fibrosis (F4)	14
Platelets counts (x10^3/mL)	124 (15-225)
Albumin (g/L)	37 (26-45)
ALAT (IU/mL)	67 (22-110)
TP (%)	77 (16-100)
Bilirubin (microM)	14 (6-291)

876

877 **B.**

	Activity score		
	A0	A1	A2
N	3	9	2
Sex	men	men	men
age	58 (42-75)	67 (40-83)	76 (71- 82)
etiology	HBV	HBV	HBV
HBV RNA (copy / mL)	8,978,257 (5,441-267,278,693)	1,303,239 (5,283-1,215,827,224)	39,499,659 (1,958-78,997,360)
Metavir fibrosis (F4)	all F4	all F4	all F4
Platelets counts (x10^3/mL)	206 (187-225)	99 (15-178)	194 (172-216)
Albumin (g/L)	NC	36 (26-44)	45
ALAT (IU/mL)	48 (24-71)	72 (35-110)	29 (22-35)
TP (%)	79 (71-87)	75 (16-100)	93 (91-95)
Bilirubin (microM)	11,5 (11-12)	16 (6-291)	10

878

879

880

881 **Suppl. Table 2. Antibodies**

Antigen	Ig Species	Cat. Number & supplier	Antibody registry (RRID) #
Beta-actin	Mouse monoclonal	sc-8432, Santa Cruz	AB_626630

Beta-tubulin	Rabbitt polyclonal	Ab6046, Abcam	AB_2210370
Alpha-SMA	Rabbitt monoclonal	1924S, Cell signalling	AB_2734735
Netrin-1	Rabbit monoclonal	Ab126729, Abcam	AB_11131145
Netrin-1	Mouse monoclonal (humanized)	NP137, Netris Pharma	AB_2811180
RIG-I	Mouse monoclonal	sc-376845, Santa Cruz	AB_2732794
PDI (P4HB)	Mouse monoclonal	sc-74551, Santa Cruz	AB_2156462
PD1 (P4HB)	Rabbit monoclonal	Ab2792, Abcam	AB_303304
Caspase-3	Rabbit polyclonal	9662, Cell Signaling	AB_331439
CD11b	Rat IgG2b, κ	BLE101206	AB_215609
CD68	Rat IgG2a	BLE137029	N/A
F4/80	Rat IgG2a, κ	BLE123135	N/A
Ly6C	Rat IgG2c, κ	BLE128017	N/A
Ly6G	Rat IgGa, κ	BLE127613	AB_2573503
CD38	Rat IgG2a, κ	BLE102720	AB_10128557
Staufen-1	Rabbit polyclonal Mouse monoclonal	Ab73478, Abcam TA811475, Origene	AB_10712675 ND
Rabbitt isotype control	Rabbit IgG	Ab172730, Abcam	AB_2687931
Human isotype control	Mouse IgG1 (humanized)	NP001, Netris Pharma	N/A
Anti-mouse-HRP	Goat polyclonal	A4416, Sigma	AB_258167
Anti-Rabbit-HRP	Goat polyclonal	A6154, Sigma	AB_258284

Anti-rabbit-Alexa 488	Donkey polyclonal	A21206, Invitrogen	AB_2535792
Anti-mouse 594	Goat monoclonal	A11032, Invitrogen	AB_2534091

882

883 **Suppl. Table 3**

Target	**Reference**	**Provider**	**Cat. #**
N/A (Ctrl siRNA)	SiC001	Sigma	SiC001
STAU1	Si00734902	Qiagen	3407629
STAU1	Si04231584	Qiagen	3407629
STAU1	Si04269335	Qiagen	3407629
STAU1	Si04272387	Qiagen	3407629

884

885 **Suppl. Table 4. Human and mouse qPCR primers**

Gene symbol	**Genbank acc. #**	**Primer sequences (5'-3', F/R)**	**PCR conditions**	**Amplicon length, bp**
NTN1 (human)	NM_004822.3	CTTCTGCGGCAGGCGGACAGAT ACGCGTTGCAGAGGTGGCACGA	Denaturation, 95°C; annealing, 65°C, 3-step, 10% DMSO	385
NTN1 (human)	NM_004822.3 (pre mRNA)	GGTAAAGTCCCGAACGCGG AAGTTTCGGGCGCAGGAGAG	Denaturation, 95°C; annealing, 55°C	133
GUS (human)	NM_001293105	CGTGGTTGGAGAGCTCATTTGG AA TTCCCCAGCACTCTCGTCGGT	Denaturation, 95°C; annealing, 55°C	72
ND1 (human)	Mitochondrial DNA	CCCTACTTCTAACCTCCCTGTTC TTAT CATAGGAGGTGTATGAGTTGGTC GTA	Denaturation, 95°C; annealing, 60°C	82

ATP6 (human)	Mitochondrial DNA	CATTTACACCAACCACCCAACTATC CGAAAGCCTATAATCACTGTGCC	Denaturation, 95°C; annealing, 60°C	82
C11ORF58 (human)	NM_014267.6	GGACTTGGCTTCAGTGAGGT TCAGGTGAATCATCATCGTCA	Denaturation, 95°C; annealing, 60°C	86
MDM2 (human)	NM_002392.6	CATGCCTGCCCACTTTAGA GGAGGCTCCCAACTGCTT	Denaturation, 95°C; annealing, 60°C	62
NTN1 (mouse)	NM_008744.2	CCTGTCACCTCTGCAACTCT TGTGCGGGTTATTGAGGTCG	Denaturation, 95°C; annealing, 55°C	78
GUS (mouse)	NM_010368.1	GTGGTATGAACGGGAAGCAAT AACTGCATAATAATGGGCACTGT	Denaturation, 95°C; annealing, 55°C	97
IL6 (mouse)	NM_031168	TCTATACCACTTCACAAGTCGGA GAATTGCCATTGCACAACTCTTT	Denaturation, 95°C; annealing, 60°C	88
CXCL10 (mouse)	NM_021274	CAAAGTGCTGCCGTCATTTT CTCAACACGTGGGCAGGATA	Denaturation, 95°C; annealing, 60°C	177
CCL2 (mouse)	NM_011333	CAGTTAACGCCCCACTCACC ACAGCTTCTTTGGGACACCT	Denaturation, 95°C; annealing, 60°C	112
IL1B (mouse)	NM_008361	TGATGTGCTGCTGCGAGATT TGCCACCTTTTGACAGTGATG	Denaturation, 95°C;	138

			annealing, 60°C	
KC (mouse)	NM_008176.3	CCATGGCTGGGATTCACCTC CAAGGGAGCTTCAGGGTCAA	Denaturation, 95°C; annealing, 60°C	58
MIP2 (mouse)	NM_009140.2	GCAAACTTTTTGACCGCCCT TCCAGAGCTTGAGTGTGACG	Denaturation, 95°C; annealing, 60°C	86
IL12B (mouse)	NM_008352	TGGTTTGCCATCGTTTTGCTG ACAGGTGAGGTTCACTGTTTCT	Denaturation, 95°C; annealing, 60°C	60
IL15 (mouse)	NM_001254747.1	CATCCATCTCGTGCTACTTGTG GCCTCTGTTTTAGGGAGACCT	Denaturation, 95°C; annealing, 60°C	112
IL4 (mouse)	NM_021283	GGTCTCAACCCCCAGCTAGT GCCGATGATCTCTCTCAAGTGAT	Denaturation, 95°C; annealing, 60°C	102
IL10 (mouse)	NM_010548	GCTGGACAACATACTGCTAACC ATTTCCGATAAGGCTTGGCAA	Denaturation, 95°C; annealing, 60°C	78
TGFB (mouse)	NM_011577	GAGCCCGAAGCGGACTACTA TGGTTTTCTCATAGATGGCGTTG	Denaturation, 95°C; annealing, 60°C	82

886

887

888 **Suppl. Table 5**

889

NTN1 5'UTR sequence (NM_004822, GenBank acc. # NM_004822, 5'-3')

ACUCCCAGCGCGAGUGGCGGCGGCGGCGGAGCCUUCGGGGGCGAGCGCGCGUGU GUGUGAGUGCGCGCCGGCCAGCGCGCCUUCUGCGGCAGGCGGACAGAUCCUCGG CGCGGCAGGGCCGGGGCAAGCUGGACGCAGCAUGAUGCGCGCAGUGUGGGAGGC GCUGGCGGCGCUGGCGGCGGUGGCGUGCCUGGUGGGCGCGGUGCGCGGCGGGC CCGGGCUCAGCAUGUUCGCGGGCCAGGCGGCGCAGCCCGAUCCCUGCUCGGACG AGAACGGCCACCCGCGCCGCUGCAUCCCGGACUUUGUCAAUGCGGCCUUCGGCAA GGUU
HBV epsilon loop (Genotype ayw, GenBank acc. # NC_003977.2, 5'-3') CUUGUUCAUGUCCUACUGUUCAAGCCUCCAAGCUGUGCCUUGGGUGGCUUUGGG GCAUGGACAUCC

Suppl. Table 6

CRISPR_CTRL_NEG_guide1	GTATTACTGATATTGGTGGG	lentiCRISPRv2 Puro
CRISPR_CTRL_NEG_guide1	CCCACCAATATCAGTAATAC	
CRISPR_CTRL_NEG_guide2	CCATCACCGATCGTGAGCCT	lentiCRISVPv2 Blast
CRISPR_CTRL_NEG_guide2	AGGCTCACGATCGGTGATGG	

CRISPR_NTN1_target_guide1	CGAACGCGGACTTTCCGGCG	lentiCRISPRv2 Puro
CRISPR_NTN1_target_guide1	CGCCGGAAAGTCCGCGTTCG	
CRISPR_NTN1_target_guide2	GCGCGACTCGTACTTCTACG	lentiCRISVPv2 Blast
CRISPR_NTN1_target_guide2	CGTAGAAGTACGAGTCGCGC	

896 **References**

897

898 1. El-Serag HB. Epidemiology of viral hepatitis and hepatocellular carcinoma.
899 Gastroenterology. 2012;142(6):1264-73 e1. Epub 2012/04/28. doi:
900 10.1053/j.gastro.2011.12.061. PubMed PMID: 22537432; PubMed Central PMCID:
901 PMC3338949.
902 2. Lee UE, Friedman SL. Mechanisms of hepatic fibrogenesis. Best Pract Res Clin
903 Gastroenterol. 2011;25(2):195-206. Epub 2011/04/19. doi:
904 10.1016/j.bpg.2011.02.005. PubMed PMID: 21497738; PubMed Central PMCID:
905 PMC3079877.
906 3. Serafini T, Kennedy TE, Galko MJ, Mirzayan C, Jessell TM, Tessier-Lavigne M.
907 The netrins define a family of axon outgrowth-promoting proteins homologous to C.
908 elegans UNC-6. Cell. 1994;78(3):409-24. Epub 1994/08/12. PubMed PMID: 8062384.
909 4. Mazelin L, Bernet A, Bonod-Bidaud C, Pays L, Arnaud S, Gespach C, et al.
910 Netrin-1 controls colorectal tumorigenesis by regulating apoptosis. Nature.
911 2004;431(7004):80-4. Epub 2004/09/03. doi: 10.1038/nature02788. PubMed PMID:
912 15343335.
913 5. Fitamant J, Guenebeaud C, Coissieux MM, Guix C, Treilleux I, Scoazec JY, et
914 al. Netrin-1 expression confers a selective advantage for tumor cell survival in
915 metastatic breast cancer. Proceedings of the National Academy of Sciences of the
916 United States of America. 2008;105(12):4850-5. Epub 2008/03/21. doi:
917 10.1073/pnas.0709810105. PubMed PMID: 18353983; PubMed Central PMCID:
918 PMC2290782.
919 6. Paradisi A, Maisse C, Bernet A, Coissieux MM, Maccarrone M, Scoazec JY, et
920 al. NF-kappaB regulates netrin-1 expression and affects the conditional tumor
921 suppressive activity of the netrin-1 receptors. Gastroenterology. 2008;135(4):1248-57.
922 Epub 2008/08/12. doi: 10.1053/j.gastro.2008.06.080. PubMed PMID: 18692059.
923 7. Dumartin L, Quemener C, Laklai H, Herbert J, Bicknell R, Bousquet C, et al.
924 Netrin-1 mediates early events in pancreatic adenocarcinoma progression, acting on
925 tumor and endothelial cells. Gastroenterology. 2010;138(4):1595-606, 606 e1-8. Epub
926 2010/01/19. doi: 10.1053/j.gastro.2009.12.061. PubMed PMID: 20080097.
927 8. Plissonnier ML, Lahlali T, Raab M, Michelet M, Romero-Lopez C, Rivoire M, et
928 al. Reciprocal antagonism between the netrin-1 receptor uncoordinated-phenotype-5A
929 (UNC5A) and the hepatitis C virus. Oncogene. 2017;36(48):6712-24. Epub
930 2017/08/08. doi: 10.1038/onc.2017.271. PubMed PMID: 28783179.
931 9. Plissonnier ML, Lahlali T, Michelet M, Lebosse F, Cottarel J, Beer M, et al.
932 Epidermal Growth Factor Receptor-Dependent Mutual Amplification between Netrin-1
933 and the Hepatitis C Virus. PLoS Biol. 2016;14(3):e1002421. Epub 2016/04/01. doi:
934 10.1371/journal.pbio.1002421. PubMed PMID: 27031829.
935 10. Llambi F, Causeret F, Bloch-Gallego E, Mehlen P. Netrin-1 acts as a survival
936 factor via its receptors UNC5H and DCC. The EMBO journal. 2001;20(11):2715-22.
937 Epub 2001/06/02. doi: 10.1093/emboj/20.11.2715. PubMed PMID: 11387206;
938 PubMed Central PMCID: PMC125255.
939 11. Thiebault K, Mazelin L, Pays L, Llambi F, Joly MO, Scoazec JY, et al. The netrin-
940 1 receptors UNC5H are putative tumor suppressors controlling cell death commitment.
941 Proceedings of the National Academy of Sciences of the United States of America.
942 2003;100(7):4173-8. Epub 2003/03/26. doi: 10.1073/pnas.0738063100. PubMed
943 PMID: 12655055; PubMed Central PMCID: PMC153067.
944 12. Llambi F, Lourenco FC, Gozuacik D, Guix C, Pays L, Del Rio G, et al. The
945 dependence receptor UNC5H2 mediates apoptosis through DAP-kinase. The EMBO

946 journal. 2005;24(6):1192-201. Epub 2005/02/25. doi: 10.1038/sj.emboj.7600584.
947 PubMed PMID: 15729359; PubMed Central PMCID: PMC556396.
948 13. Mille F, Llambi F, Guix C, Delloye-Bourgeois C, Guenebeaud C, Castro-
949 Obregon S, et al. Interfering with multimerization of netrin-1 receptors triggers tumor
950 cell death. Cell death and differentiation. 2009;16(10):1344-51. Epub 2009/06/23. doi:
951 10.1038/cdd.2009.75. PubMed PMID: 19543238; PubMed Central PMCID:
952 PMC2841642.
953 14. Guenebeaud C, Goldschneider D, Castets M, Guix C, Chazot G, Delloye-
954 Bourgeois C, et al. The dependence receptor UNC5H2/B triggers apoptosis via PP2A-
955 mediated dephosphorylation of DAP kinase. Molecular cell. 2010;40(6):863-76. Epub
956 2010/12/22. doi: 10.1016/j.molcel.2010.11.021. PubMed PMID: 21172653.
957 15. Paradisi A, Creveaux M, Gibert B, Devailly G, Redoulez E, Neves D, et al.
958 Combining chemotherapeutic agents and netrin-1 interference potentiates cancer cell
959 death. EMBO Mol Med. 2013;5(12):1821-34. Epub 2013/12/03. doi:
960 10.1002/emmm.201302654. PubMed PMID: 24293316.
961 16. Lahlali T, Plissonnier ML, Romero-Lopez C, Michelet M, Ducarouge B, Berzal-
962 Herranz A, et al. Netrin-1 Protects Hepatocytes Against Cell Death Through Sustained
963 Translation During the Unfolded Protein Response. Cell Mol Gastroenterol Hepatol.
964 2016;2(3):281-301 e9. Epub 2017/02/09. doi: 10.1016/j.jcmgh.2015.12.011. PubMed
965 PMID: 28174720; PubMed Central PMCID: PMCPMC5042567.
966 17. Asselah T, Bieche I, Mansouri A, Laurendeau I, Cazals-Hatem D, Feldmann G,
967 et al. In vivo hepatic endoplasmic reticulum stress in patients with chronic hepatitis C.
968 J Pathol. 2010;221(3):264-74. Epub 2010/06/09. doi: 10.1002/path.2703. PubMed
969 PMID: 20527020.
970 18. Joyce MA, Walters KA, Lamb SE, Yeh MM, Zhu LF, Kneteman N, et al. HCV
971 induces oxidative and ER stress, and sensitizes infected cells to apoptosis in
972 SCID/Alb-uPA mice. PLoS Pathog. 2009;5(2):e1000291. Epub 2009/02/27. doi:
973 10.1371/journal.ppat.1000291. PubMed PMID: 19242562; PubMed Central PMCID:
974 PMC2647842.
975 19. Maiers JL, Malhi H. Endoplasmic Reticulum Stress in Metabolic Liver Diseases
976 and Hepatic Fibrosis. Semin Liver Dis. 2019;39(2):235-48. Epub 2019/03/27. doi:
977 10.1055/s-0039-1681032. PubMed PMID: 30912096; PubMed Central PMCID:
978 PMCPMC6530577.
979 20. Hadi T, Boytard L, Silvestro M, Alebrahim D, Jacob S, Feinstein J, et al.
980 Macrophage-derived netrin-1 promotes abdominal aortic aneurysm formation by
981 activating MMP3 in vascular smooth muscle cells. Nat Commun. 2018;9(1):5022. Epub
982 2018/11/28. doi: 10.1038/s41467-018-07495-1. PubMed PMID: 30479344; PubMed
983 Central PMCID: PMCPMC6258757.
984 21. Mediero A, Wilder T, Ramkhelawon B, Moore KJ, Cronstein BN. Netrin-1 and
985 its receptor Unc5b are novel targets for the treatment of inflammatory arthritis. FASEB
986 J. 2016;30(11):3835-44. Epub 2016/11/03. doi: 10.1096/fj.201600615R. PubMed
987 PMID: 27502509; PubMed Central PMCID: PMCPMC5067256.
988 22. van Gils JM, Derby MC, Fernandes LR, Ramkhelawon B, Ray TD, Rayner KJ,
989 et al. The neuroimmune guidance cue netrin-1 promotes atherosclerosis by inhibiting
990 the emigration of macrophages from plaques. Nat Immunol. 2012;13(2):136-43. Epub
991 2012/01/11. doi: 10.1038/ni.2205. PubMed PMID: 22231519; PubMed Central PMCID:
992 PMC3262880.
993 23. Rosenberger P, Schwab JM, Mirakaj V, Masekowsky E, Mager A, Morote-
994 Garcia JC, et al. Hypoxia-inducible factor-dependent induction of netrin-1 dampens

995 inflammation caused by hypoxia. Nat Immunol. 2009;10(2):195-202. Epub 2009/01/06.
996 doi: 10.1038/ni.1683. PubMed PMID: 19122655.
997 24. Mirakaj V, Thix CA, Laucher S, Mielke C, Morote-Garcia JC, Schmit MA, et al.
998 Netrin-1 dampens pulmonary inflammation during acute lung injury. Am J Respir Crit
999 Care Med. 2010;181(8):815-24. Epub 2010/01/16. doi: 10.1164/rccm.200905-
1000 0717OC. PubMed PMID: 20075388.
1001 25. Aherne CM, Collins CB, Masterson JC, Tizzano M, Boyle TA, Westrich JA, et
1002 al. Neuronal guidance molecule netrin-1 attenuates inflammatory cell trafficking during
1003 acute experimental colitis. Gut. 2012;61(5):695-705. Epub 2011/08/05. doi:
1004 10.1136/gutjnl-2011-300012. PubMed PMID: 21813473; PubMed Central PMCID:
1005 PMC3322588.
1006 26. Paradisi A, Maisse C, Coissieux MM, Gadot N, Lepinasse F, Delloye-Bourgeois
1007 C, et al. Netrin-1 up-regulation in inflammatory bowel diseases is required for colorectal
1008 cancer progression. Proceedings of the National Academy of Sciences of the United
1009 States of America. 2009;106(40):17146-51. Epub 2009/09/02. doi:
1010 10.1073/pnas.0901767106. PubMed PMID: 19721007; PubMed Central PMCID:
1011 PMC2761333.
1012 27. Grandin M, Meier M, Delcros JG, Nikodemus D, Reuten R, Patel TR, et al.
1013 Structural Decoding of the Netrin-1/UNC5 Interaction and its Therapeutical
1014 Implications in Cancers. Cancer Cell. 2016;29(2):173-85. Epub 2016/02/10. doi:
1015 10.1016/j.ccell.2016.01.001. PubMed PMID: 26859457.
1016 28. Jungermann K, Kietzmann T. Zonation of parenchymal and nonparenchymal
1017 metabolism in liver. Annu Rev Nutr. 1996;16:179-203. Epub 1996/01/01. doi:
1018 10.1146/annurev.nu.16.070196.001143. PubMed PMID: 8839925.
1019 29. Lecluyse EL, Alexandre E. Isolation and culture of primary hepatocytes from
1020 resected human liver tissue. Methods Mol Biol. 2010;640:57-82. Epub 2010/07/21. doi:
1021 10.1007/978-1-60761-688-7_3. PubMed PMID: 20645046.
1022 30. Repetto G, del Peso A, Zurita JL. Neutral red uptake assay for the estimation of
1023 cell viability/cytotoxicity. Nat Protoc. 2008;3(7):1125-31. Epub 2008/07/05. doi:
1024 10.1038/nprot.2008.75. PubMed PMID: 18600217.
1025 31. Parent R, Kolippakkam D, Booth G, Beretta L. Mammalian target of rapamycin
1026 activation impairs hepatocytic differentiation and targets genes moderating lipid
1027 homeostasis and hepatocellular growth. Cancer research. 2007;67(9):4337-45. Epub
1028 2007/05/08. doi: 10.1158/0008-5472.can-06-3640. PubMed PMID: 17483347.
1029 32. Stephens SB, Nicchitta CV. In vitro and tissue culture methods for analysis of
1030 translation initiation on the endoplasmic reticulum. Methods Enzymol. 2007;431:47-60.
1031 Epub 2007/10/10. doi: 10.1016/S0076-6879(07)31004-5. PubMed PMID: 17923230.
1032 33. Stephens SB, Dodd RD, Lerner RS, Pyhtila BM, Nicchitta CV. Analysis of mRNA
1033 partitioning between the cytosol and endoplasmic reticulum compartments of
1034 mammalian cells. Methods Mol Biol. 2008;419:197-214. Epub 2008/03/29. doi:
1035 10.1007/978-1-59745-033-1_14. PubMed PMID: 18369985.
1036 34. Casabona MG, Vandenbrouck Y, Attree I, Coute Y. Proteomic characterization
1037 of Pseudomonas aeruginosa PAO1 inner membrane. Proteomics. 2013;13(16):2419-
1038 23. Epub 2013/06/08. doi: 10.1002/pmic.201200565. PubMed PMID: 23744604.
1039 35. Tyanova S, Temu T, Cox J. The MaxQuant computational platform for mass
1040 spectrometry-based shotgun proteomics. Nat Protoc. 2016;11(12):2301-19. Epub
1041 2016/11/04. doi: 10.1038/nprot.2016.136. PubMed PMID: 27809316.
1042 36. Boncompain G, Perez F. Fluorescence-based analysis of trafficking in
1043 mammalian cells. Methods Cell Biol. 2013;118:179-94. Epub 2013/12/04. doi:
1044 10.1016/B978-0-12-417164-0.00011-2. PubMed PMID: 24295307.

1045 37. Sanjana NE, Shalem O, Zhang F. Improved vectors and genome-wide libraries
1046 for CRISPR screening. Nat Methods. 2014;11(8):783-4. Epub 2014/07/31. doi:
1047 10.1038/nmeth.3047. PubMed PMID: 25075903; PubMed Central PMCID:
1048 PMCPMC4486245.
1049 38. Bassot A, Chauvin MA, Bendridi N, Ji-Cao J, Vial G, Monnier L, et al. Regulation
1050 of Mitochondria-Associated Membranes (MAMs) by NO/sGC/PKG Participates in the
1051 Control of Hepatic Insulin Response. Cells. 2019;8(11). Epub 2019/11/17. doi:
1052 10.3390/cells8111319. PubMed PMID: 31731523; PubMed Central PMCID:
1053 PMCPMC6912364.
1054 39. Friedman SL. Hepatic stellate cells: protean, multifunctional, and enigmatic cells
1055 of the liver. Physiol Rev. 2008;88(1):125-72. Epub 2008/01/16. doi:
1056 10.1152/physrev.00013.2007. PubMed PMID: 18195085; PubMed Central PMCID:
1057 PMCPMC2888531.
1058 40. Koyama Y, Brenner DA. Liver inflammation and fibrosis. J Clin Invest.
1059 2017;127(1):55-64. Epub 2017/01/04. doi: 10.1172/JCI88881. PubMed PMID:
1060 28045404; PubMed Central PMCID: PMCPMC5199698.
1061 41. Parent R, Marion MJ, Furio L, Trepo C, Petit MA. Origin and characterization of
1062 a human bipotent liver progenitor cell line. Gastroenterology. 2004;126(4):1147-56.
1063 Epub 2004/04/02. PubMed PMID: 15057753.
1064 42. Gripon P, Rumin S, Urban S, Le Seyec J, Glaise D, Cannie I, et al. Infection of
1065 a human hepatoma cell line by hepatitis B virus. Proceedings of the National Academy
1066 of Sciences of the United States of America. 2002;99(24):15655-60. Epub 2002/11/15.
1067 doi: 10.1073/pnas.232137699. PubMed PMID: 12432097; PubMed Central PMCID:
1068 PMC137772.
1069 43. Saito T, Owen DM, Jiang F, Marcotrigiano J, Gale M, Jr. Innate immunity
1070 induced by composition-dependent RIG-I recognition of hepatitis C virus RNA. Nature.
1071 2008;454(7203):523-7. Epub 2008/06/13. doi: 10.1038/nature07106. PubMed PMID:
1072 18548002; PubMed Central PMCID: PMCPMC2856441.
1073 44. Sato S, Li K, Kameyama T, Hayashi T, Ishida Y, Murakami S, et al. The RNA
1074 sensor RIG-I dually functions as an innate sensor and direct antiviral factor for hepatitis
1075 B virus. Immunity. 2015;42(1):123-32. Epub 2015/01/06. doi:
1076 10.1016/j.immuni.2014.12.016. PubMed PMID: 25557055.
1077 45. Maire M, Parent R, Morand AL, Alotte C, Trepo C, Durantel D, et al.
1078 Characterization of the double-stranded RNA responses in human liver progenitor
1079 cells. Biochemical and biophysical research communications. 2008;368(3):556-62.
1080 Epub 2008/02/09. doi: 10.1016/j.bbrc.2008.01.123. PubMed PMID: 18258184.
1081 46. Leclere L, Rentzsch F. Repeated evolution of identical domain architecture in
1082 metazoan netrin domain-containing proteins. Genome Biol Evol. 2012;4(9):883-99.
1083 Epub 2012/07/21. doi: 10.1093/gbe/evs061. PubMed PMID: 22813778; PubMed
1084 Central PMCID: PMCPMC3516229.
1085 47. Vispe S, DeVries L, Creancier L, Besse J, Breand S, Hobson DJ, et al. Triptolide
1086 is an inhibitor of RNA polymerase I and II-dependent transcription leading
1087 predominantly to down-regulation of short-lived mRNA. Mol Cancer Ther.
1088 2009;8(10):2780-90. Epub 2009/10/08. doi: 10.1158/1535-7163.MCT-09-0549.
1089 PubMed PMID: 19808979.
1090 48. Barnault R, Lahlali T, Plissonnier ML, Romero-Lopez C, Laverdure N,
1091 Ducarouge B, et al. Hepatocellular carcinoma-associated depletion of the netrin-1
1092 receptor Uncoordinated Phenotype-5A (UNC5A) skews the hepatic unfolded protein
1093 response towards prosurvival outcomes. Biochem Biophys Res Commun.

1094 2018;495(4):2425-31. Epub 2017/12/27. doi: 10.1016/j.bbrc.2017.12.129. PubMed
1095 PMID: 29277614.
1096 49. Reid DW, Nicchitta CV. Primary role for endoplasmic reticulum-bound
1097 ribosomes in cellular translation identified by ribosome profiling. J Biol Chem.
1098 2012;287(8):5518-27. Epub 2011/12/27. doi: 10.1074/jbc.M111.312280. PubMed
1099 PMID: 22199352; PubMed Central PMCID: PMCPMC3285328.
1100 50. Chen Q, Jagannathan S, Reid DW, Zheng T, Nicchitta CV. Hierarchical
1101 regulation of mRNA partitioning between the cytoplasm and the endoplasmic reticulum
1102 of mammalian cells. Mol Biol Cell. 2011;22(14):2646-58. Epub 2011/05/27. doi:
1103 10.1091/mbc.E11-03-0239. PubMed PMID: 21613539; PubMed Central PMCID:
1104 PMCPMC3135488.
1105 51. Wickham L, Duchaine T, Luo M, Nabi IR, DesGroseillers L. Mammalian staufen
1106 is a double-stranded-RNA- and tubulin-binding protein which localizes to the rough
1107 endoplasmic reticulum. Mol Cell Biol. 1999;19(3):2220-30. Epub 1999/02/18. doi:
1108 10.1128/mcb.19.3.2220. PubMed PMID: 10022909; PubMed Central PMCID:
1109 PMCPMC84015.
1110 52. Marion RM, Fortes P, Beloso A, Dotti C, Ortin J. A human sequence homologue
1111 of Staufen is an RNA-binding protein that is associated with polysomes and localizes
1112 to the rough endoplasmic reticulum. Mol Cell Biol. 1999;19(3):2212-9. Epub
1113 1999/02/18. doi: 10.1128/mcb.19.3.2212. PubMed PMID: 10022908; PubMed Central
1114 PMCID: PMCPMC84014.
1115 53. Dugre-Brisson S, Elvira G, Boulay K, Chatel-Chaix L, Mouland AJ,
1116 DesGroseillers L. Interaction of Staufen1 with the 5' end of mRNA facilitates translation
1117 of these RNAs. Nucleic Acids Res. 2005;33(15):4797-812. Epub 2005/08/30. doi:
1118 10.1093/nar/gki794. PubMed PMID: 16126845; PubMed Central PMCID:
1119 PMCPMC1193567.
1120 54. Ricci EP, Kucukural A, Cenik C, Mercier BC, Singh G, Heyer EE, et al. Staufen1
1121 senses overall transcript secondary structure to regulate translation. Nat Struct Mol
1122 Biol. 2014;21(1):26-35. Epub 2013/12/18. doi: 10.1038/nsmb.2739. PubMed PMID:
1123 24336223; PubMed Central PMCID: PMCPMC4605437.
1124 55. Furic L, Maher-Laporte M, DesGroseillers L. A genome-wide approach identifies
1125 distinct but overlapping subsets of cellular mRNAs associated with Staufen1- and
1126 Staufen2-containing ribonucleoprotein complexes. RNA. 2008;14(2):324-35. Epub
1127 2007/12/21. doi: 10.1261/rna.720308. PubMed PMID: 18094122; PubMed Central
1128 PMCID: PMCPMC2212254.
1129 56. de Lucas S, Oliveros JC, Chagoyen M, Ortin J. Functional signature for the
1130 recognition of specific target mRNAs by human Staufen1 protein. Nucleic Acids Res.
1131 2014;42(7):4516-26. Epub 2014/01/29. doi: 10.1093/nar/gku073. PubMed PMID:
1132 24470147; PubMed Central PMCID: PMCPMC3985646.
1133 57. Villace P, Marion RM, Ortin J. The composition of Staufen-containing RNA
1134 granules from human cells indicates their role in the regulated transport and translation
1135 of messenger RNAs. Nucleic Acids Res. 2004;32(8):2411-20. Epub 2004/05/04. doi:
1136 10.1093/nar/gkh552. PubMed PMID: 15121898; PubMed Central PMCID:
1137 PMCPMC419443.
1138 58. Kohrmann M, Luo M, Kaether C, DesGroseillers L, Dotti CG, Kiebler MA.
1139 Microtubule-dependent recruitment of Staufen-green fluorescent protein into large
1140 RNA-containing granules and subsequent dendritic transport in living hippocampal
1141 neurons. Mol Biol Cell. 1999;10(9):2945-53. Epub 1999/09/03. doi:
1142 10.1091/mbc.10.9.2945. PubMed PMID: 10473638; PubMed Central PMCID:
1143 PMCPMC25535.

1144 59. Fang J, Pietzsch C, Ramanathan P, Santos RI, Ilinykh PA, Garcia-Blanco MA,
1145 et al. Staufen1 Interacts with Multiple Components of the Ebola Virus
1146 Ribonucleoprotein and Enhances Viral RNA Synthesis. mBio. 2018;9(5). Epub
1147 2018/10/12. doi: 10.1128/mBio.01771-18. PubMed PMID: 30301857; PubMed Central
1148 PMCID: PMCPMC6178623.
1149 60. Taketa K, Pogell BM. Allosteric Inhibition of Rat Liver Fructose 1,6-
1150 Diphosphatase by Adenosine 5'-Monophosphate. J Biol Chem. 1965;240:651-62.
1151 Epub 1965/02/01. PubMed PMID: 14275118.
1152 61. Schlegel M, Kohler D, Korner A, Granja T, Straub A, Giera M, et al. The
1153 neuroimmune guidance cue netrin-1 controls resolution programs and promotes liver
1154 regeneration. Hepatology. 2015. Epub 2015/11/18. doi: 10.1002/hep.28347. PubMed
1155 PMID: 26573873.
1156 62. El-Serag HB, Marrero JA, Rudolph L, Reddy KR. Diagnosis and treatment of
1157 hepatocellular carcinoma. Gastroenterology. 2008;134(6):1752-63. Epub 2008/05/13.
1158 doi: 10.1053/j.gastro.2008.02.090
1159 S0016-5085(08)00426-5 [pii]. PubMed PMID: 18471552.
1160 63. Umemura A, Park EJ, Taniguchi K, Lee JH, Shalapour S, Valasek MA, et al.
1161 Liver damage, inflammation, and enhanced tumorigenesis after persistent mTORC1
1162 inhibition. Cell Metab. 2014;20(1):133-44. Epub 2014/06/10. doi:
1163 10.1016/j.cmet.2014.05.001. PubMed PMID: 24910242; PubMed Central PMCID:
1164 PMCPMC4079758.
1165 64. He G, Dhar D, Nakagawa H, Font-Burgada J, Ogata H, Jiang Y, et al.
1166 Identification of liver cancer progenitors whose malignant progression depends on
1167 autocrine IL-6 signaling. Cell. 2013;155(2):384-96. Epub 2013/10/15. doi:
1168 10.1016/j.cell.2013.09.031. PubMed PMID: 24120137; PubMed Central PMCID:
1169 PMCPMC4015514.
1170 65. Park EJ, Lee JH, Yu GY, He G, Ali SR, Holzer RG, et al. Dietary and genetic
1171 obesity promote liver inflammation and tumorigenesis by enhancing IL-6 and TNF
1172 expression. Cell. 2010;140(2):197-208. Epub 2010/02/10. doi:
1173 10.1016/j.cell.2009.12.052. PubMed PMID: 20141834; PubMed Central PMCID:
1174 PMCPMC2836922.
1175 66. Naugler WE, Sakurai T, Kim S, Maeda S, Kim K, Elsharkawy AM, et al. Gender
1176 disparity in liver cancer due to sex differences in MyD88-dependent IL-6 production.
1177 Science. 2007;317(5834):121-4. Epub 2007/07/07. doi: 10.1126/science.1140485.
1178 PubMed PMID: 17615358.
1179 67. Odom DT, Zizlsperger N, Gordon DB, Bell GW, Rinaldi NJ, Murray HL, et al.
1180 Control of pancreas and liver gene expression by HNF transcription factors. Science.
1181 2004;303(5662):1378-81. Epub 2004/02/28. doi: 10.1126/science.1089769. PubMed
1182 PMID: 14988562; PubMed Central PMCID: PMCPMC3012624.
1183 68. Knight JRP, Alexandrou C, Skalka GL, Vlahov N, Pennel K, Officer L, et al. MNK
1184 inhibition sensitizes KRAS-mutant colorectal cancer to mTORC1 inhibition by reducing
1185 eIF4E phosphorylation and c-MYC expression. Cancer Discov. 2020. Epub
1186 2020/12/18. doi: 10.1158/2159-8290.CD-20-0652. PubMed PMID: 33328217.
1187 69. Boussemart L, Malka-Mahieu H, Girault I, Allard D, Hemmingsson O, Tomasic
1188 G, et al. eIF4F is a nexus of resistance to anti-BRAF and anti-MEK cancer therapies.
1189 Nature. 2014;513(7516):105-9. Epub 2014/08/01. doi: 10.1038/nature13572. PubMed
1190 PMID: 25079330.
1191 70. Parent R, Beretta L. Translational control plays a prominent role in the
1192 hepatocytic differentiation of HepaRG liver progenitor cells. Genome Biol.

2008;9(1):R19. Epub 2008/01/29. doi: 10.1186/gb-2008-9-1-r19. PubMed PMID: 18221535; PubMed Central PMCID: PMC2395229.
71. Sahin F, Kannangai R, Adegbola O, Wang J, Su G, Torbenson M. mTOR and P70 S6 kinase expression in primary liver neoplasms. Clin Cancer Res. 2004;10(24):8421-5. Epub 2004/12/30. doi: 10.1158/1078-0432.CCR-04-0941. PubMed PMID: 15623621.
72. Lahlali T, Plissonnier ML, Romero-López C, Michelet M, Ducarouge B, Berzal-Herranz A, et al. Netrin-1 Protects Hepatocytes Against Cell Death Through Sustained Translation During the Unfolded Protein Response. Cell Mol Gastroenterol Hepatol. 2016;2(3):281-301.e9. Epub 2017/02/09. doi: 10.1016/j.jcmgh.2015.12.011. PubMed PMID: 28174720; PubMed Central PMCID: PMCPMC5042567.
73. Xu TP, Wang YF, Xiong WL, Ma P, Wang WY, Chen WM, et al. E2F1 induces TINCR transcriptional activity and accelerates gastric cancer progression via activation of TINCR/STAU1/CDKN2B signaling axis. Cell Death Dis. 2017;8(6):e2837. Epub 2017/06/02. doi: 10.1038/cddis.2017.205. PubMed PMID: 28569791; PubMed Central PMCID: PMCPMC5520882.
74. Xu F, Li CH, Wong CH, Chen GG, Lai PBS, Shao S, et al. Genome-Wide Screening and Functional Analysis Identifies Tumor Suppressor Long Noncoding RNAs Epigenetically Silenced in Hepatocellular Carcinoma. Cancer Res. 2019;79(7):1305-17. Epub 2019/02/06. doi: 10.1158/0008-5472.CAN-18-1659. PubMed PMID: 30718359.
75. He G, Karin M. NF-kappaB and STAT3 - key players in liver inflammation and cancer. Cell Res. 2011;21(1):159-68. Epub 2010/12/29. doi: 10.1038/cr.2010.183. PubMed PMID: 21187858; PubMed Central PMCID: PMCPMC3193410.
76. Mehlen P, Delloye-Bourgeois C, Chedotal A. Novel roles for Slits and netrins: axon guidance cues as anticancer targets? Nature reviews Cancer. 2011;11(3):188-97. Epub 2011/02/18. doi: 10.1038/nrc3005. PubMed PMID: 21326323.
77. Gao R, Peng X, Perry C, Sun H, Ntokou A, Ryu C, et al. Macrophage-derived netrin-1 drives adrenergic nerve-associated lung fibrosis. J Clin Invest. 2021;131(1). Epub 2021/01/05. doi: 10.1172/JCI136542. PubMed PMID: 33393489; PubMed Central PMCID: PMCPMC7773383.
78. Romanowski T, Sikorska K, Bielawski KP. GUS and PMM1 as suitable reference genes for gene expression analysis in the liver tissue of patients with chronic hepatitis. Med Sci Monit. 2008;14(7):BR147-52. Epub 2008/07/02. PubMed PMID: 18591914.

Figure 1

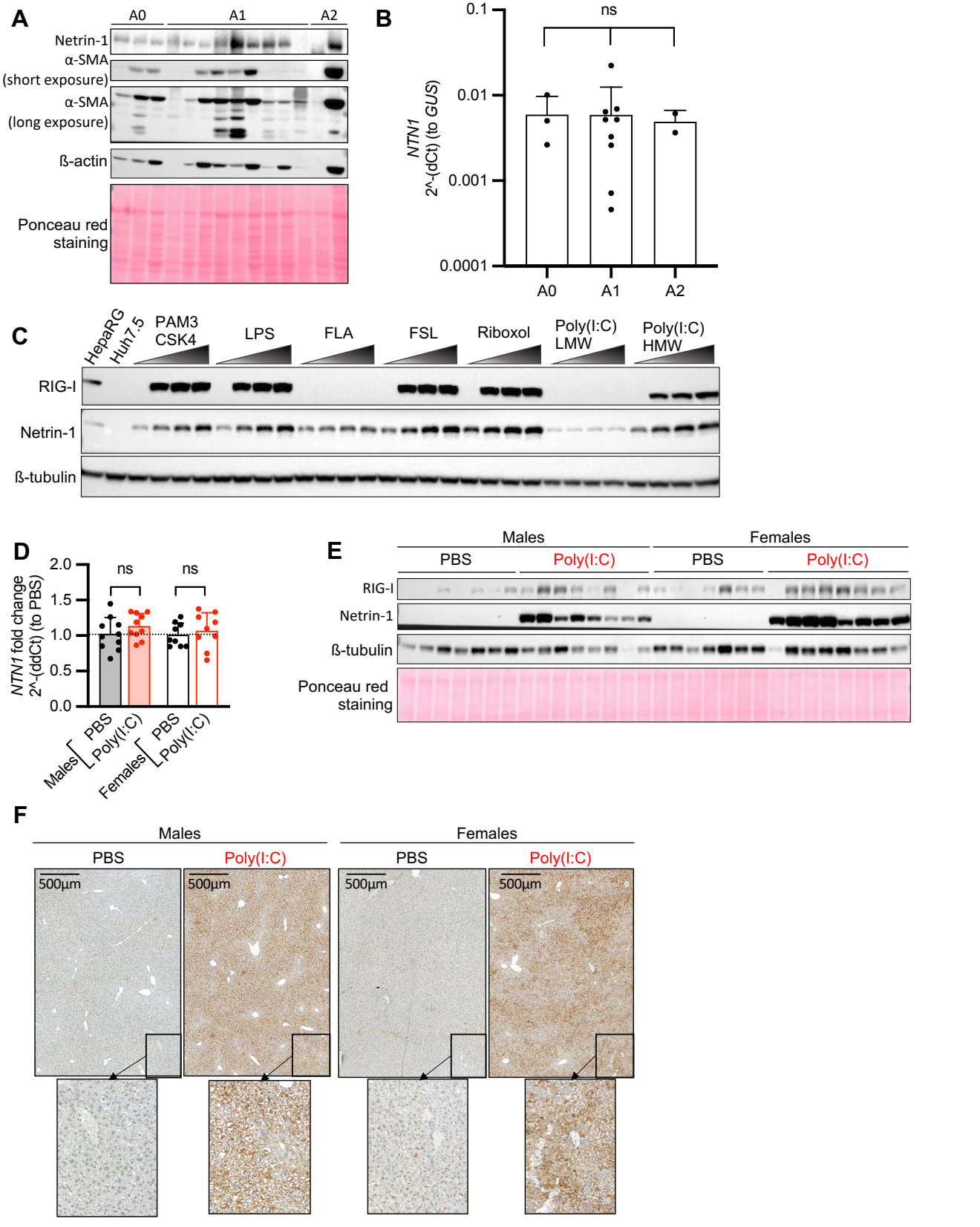
A
A0
A1
A2
Netrin-1
α-SMA
(short exposure)
α-SMA
(long exposure)
ß-actin
Ponceau red
staining
B
ns
0.1
0.01
0.001
0.0001
NTN1
2^-(dCt) (to GUS)
A0
A1
A2
C
HepaRG
Huh7.5
PAM3
CSK4
LPS
FLA
FSL
Riboxol
Poly(I:C)
LMW
Poly(I:C)
HMW
RIG-I
Netrin-1
ß-tubulin
D
ns
ns
2.0
1.5
1.0
0.5
0.0
NTN1 fold change
2^-(ddCt) (to PBS)
PBS
Poly(I:C)
Males
PBS
Poly(I:C)
Females
E
Males
Females
PBS
Poly(I:C)
PBS
Poly(I:C)
RIG-I
Netrin-1
ß-tubulin
Ponceau red
staining
F
Males
Females
PBS
Poly(I:C)
PBS
Poly(I:C)
500µm
500µm
500µm
500µm

Figure 2

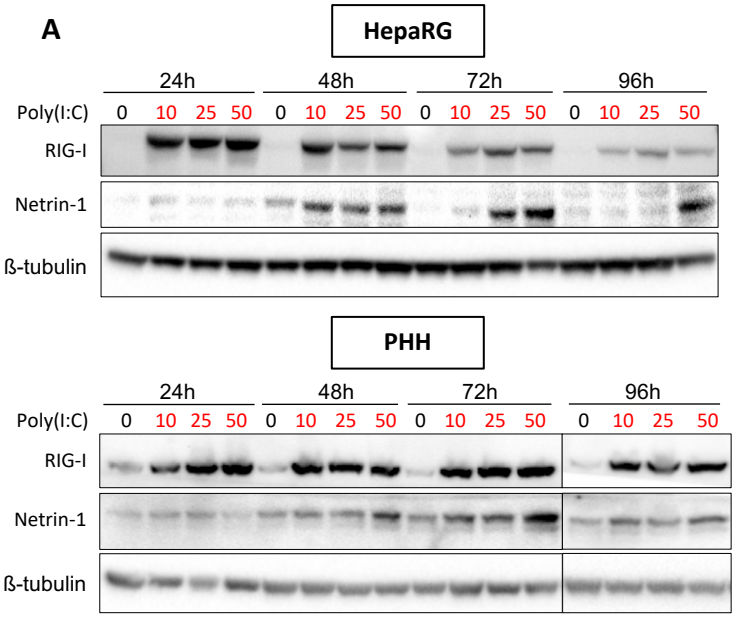
A
HepaRG
24h
48h
72h
96h
Poly(I:C)
0 10 25 50 0 10 25 50 0 10 25 50 0 10 25 50
RIG-I
Netrin-1
ß-tubulin
PHH
24h
48h
72h
96h
Poly(I:C)
0 10 25 50 0 10 25 50 0 10 25 50 0 10 25 50
RIG-I
Netrin-1
ß-tubulin

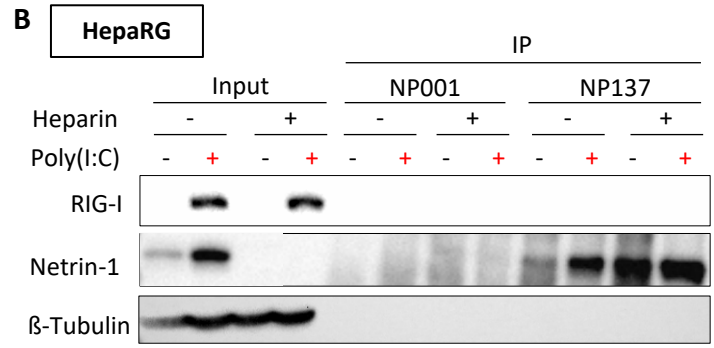
B
HepaRG
IP
Input
NP001
NP137
Heparin
- + - + - +
Poly(I:C)
- + - + - + - + - + - +
RIG-I
Netrin-1
ß-Tubulin

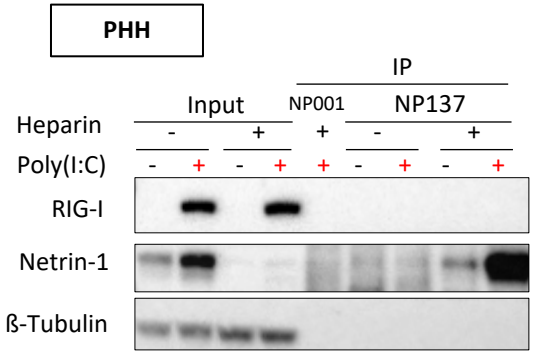
PHH
IP
Input
NP001
NP137
Heparin
- + + - +
Poly(I:C)
- + - + + - + - +
RIG-I
Netrin-1
ß-Tubulin

Figure 3

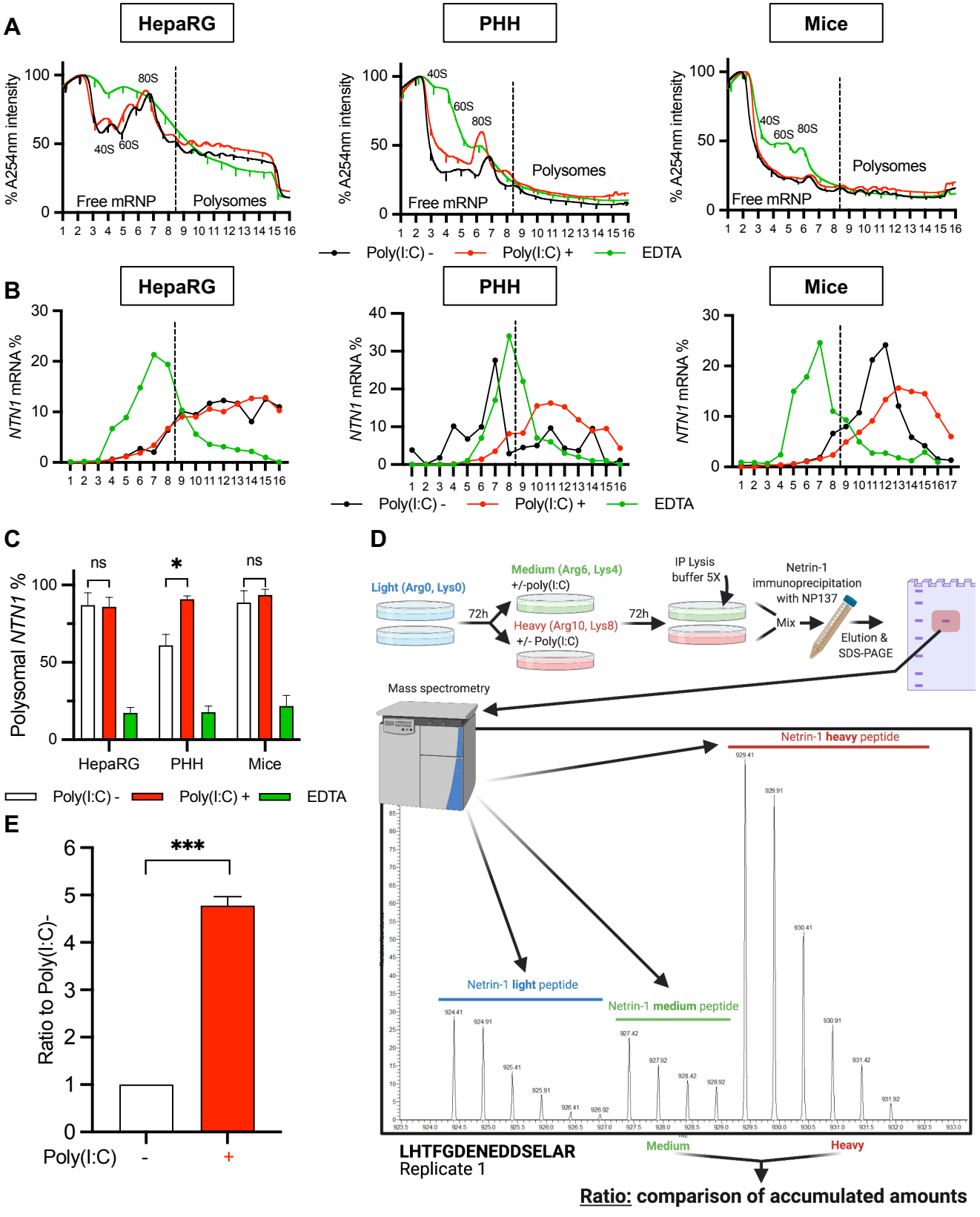
A
HepaRG
PHH
Mice
% A254nm intensity
80S
40S
60S
Free mRNP
Polysomes
Poly(I:C) -
Poly(I:C) +
EDTA
B
NTN1 mRNA %
C
Polysomal NTN1 %
ns
*
HepaRG
PHH
Mice
D
Light (Arg0, Lys0)
Medium (Arg6, Lys4)
+/-poly(I:C)
Heavy (Arg10, Lys8)
+/- Poly(I:C)
72h
IP Lysis buffer 5X
Netrin-1 immunoprecipitation with NP137
Mix
Elution & SDS-PAGE
Mass spectrometry
Netrin-1 heavy peptide
Netrin-1 light peptide
Netrin-1 medium peptide
LHTFGDENEDDSELAR
Replicate 1
Medium
Heavy
Ratio: comparison of accumulated amounts
E
***
Ratio to Poly(I:C)-
Poly(I:C)

Figure 4

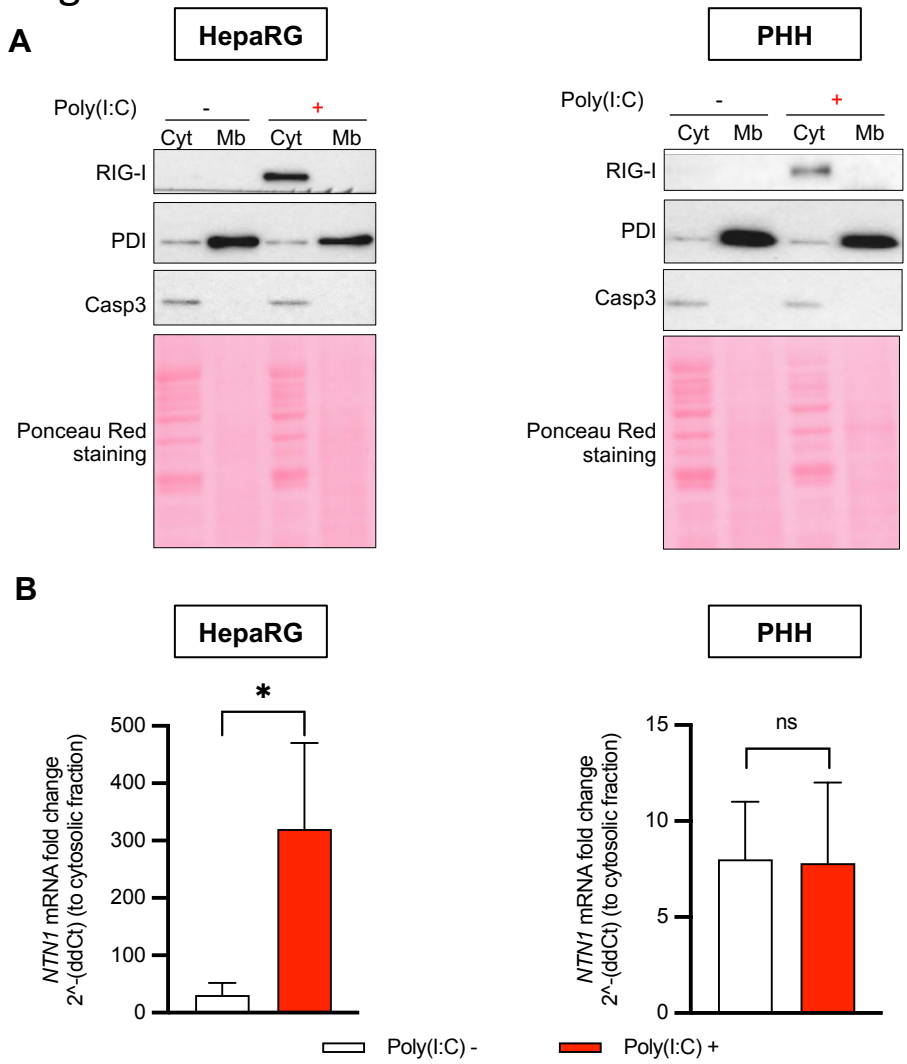
A
HepaRG
PHH
Poly(I:C)
-
+
Cyt
Mb
RIG-I
PDI
Casp3
Ponceau Red staining
B
*
ns
NTN1 mRNA fold change 2^-(ddCt) (to cytosolic fraction)
500
400
300
200
100
0
15
10
5
Poly(I:C) -
Poly(I:C) +

Figure 5

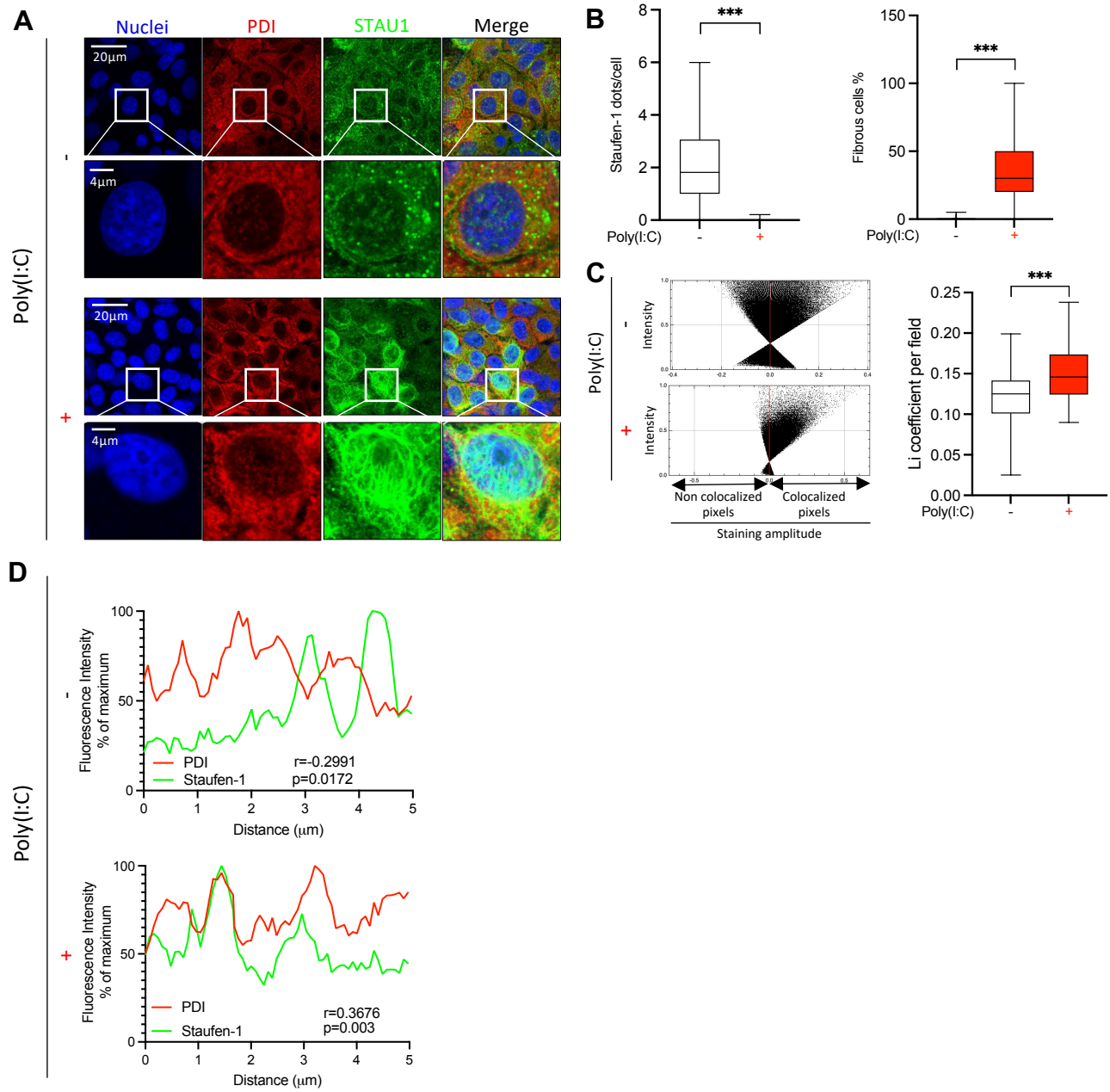
A
Nuclei
PDI
STAU1
Merge
20µm
4µm
Poly(I:C)
-
+
B
Staufen-1 dots/cell
***
Poly(I:C)
Fibrous cells %
C
Intensity
Non colocalized pixels
Colocalized pixels
Staining amplitude
Li coefficient per field
D
Fluorescence Intensity % of maximum
PDI
Staufen-1
r=-0.2991
p=0.0172
Distance (µm)
r=0.3676
p=0.003

Figure 6

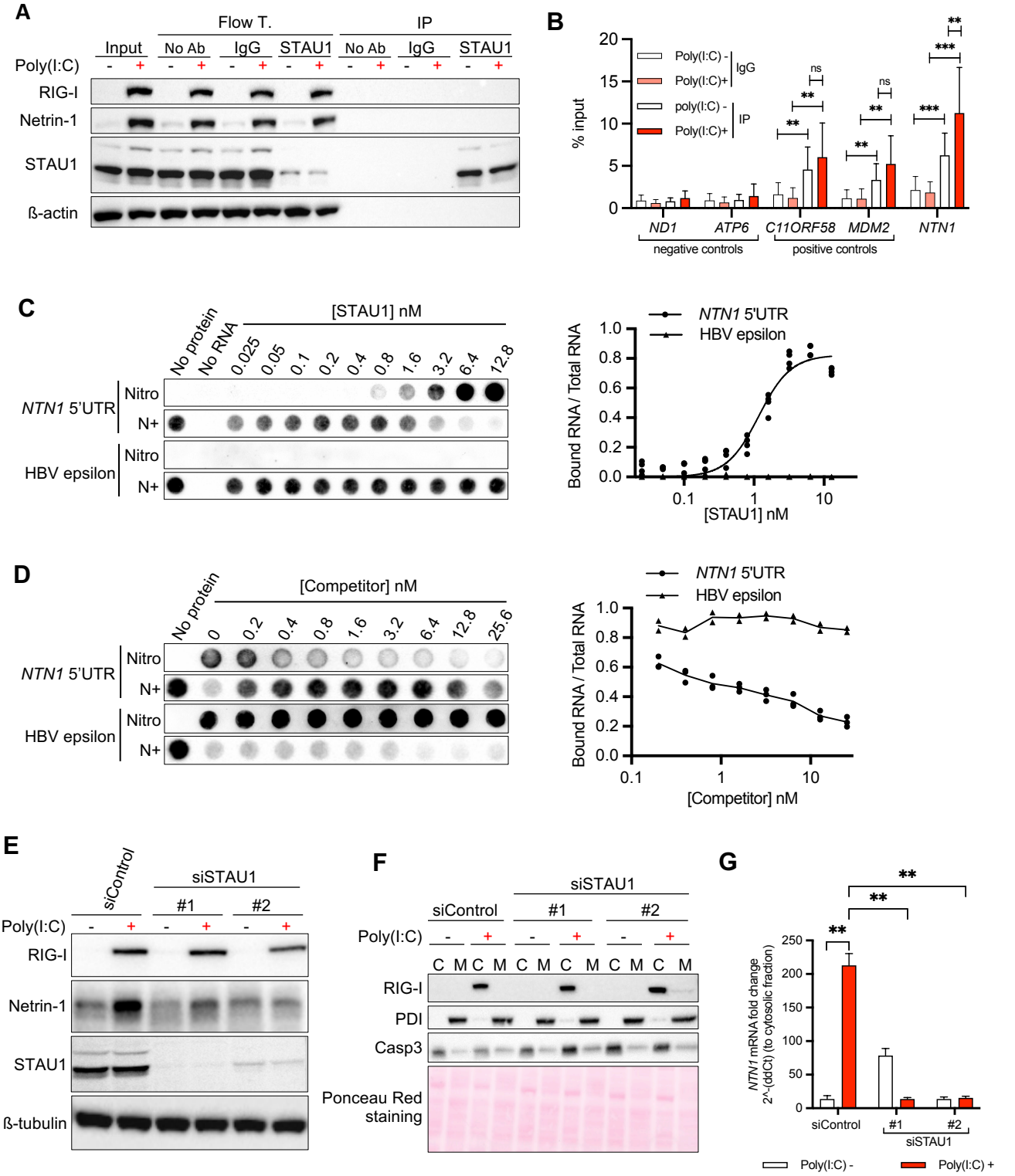
A
Flow T.
IP
Input
No Ab
IgG
STAU1
No Ab
IgG
STAU1
Poly(I:C)
RIG-I
Netrin-1
STAU1
ß-actin
B
% input
Poly(I:C) -
Poly(I:C)+
IgG
poly(I:C) -
Poly(I:C)+
IP
ns
**
***
ND1
ATP6
C11ORF58
MDM2
NTN1
negative controls
positive controls
C
[STAU1] nM
No protein
No RNA
0.025
0.05
0.1
0.2
0.4
0.8
1.6
3.2
6.4
12.8
NTN1 5'UTR
HBV epsilon
Nitro
N+
Bound RNA / Total RNA
[STAU1] nM
D
[Competitor] nM
No protein
0
0.2
0.4
0.8
1.6
3.2
6.4
12.8
25.6
[Competitor] nM
E
siControl
siSTAU1
#1
#2
Poly(I:C)
RIG-I
Netrin-1
STAU1
ß-tubulin
F
siControl
siSTAU1
#1
#2
Poly(I:C)
C M C M C M C M C M C M
RIG-I
PDI
Casp3
Ponceau Red staining
G
NTN1 mRNA fold change 2^-(ddCt) (to cytosolic fraction)
siControl
#1
#2
siSTAU1
Poly(I:C) -
Poly(I:C) +

Figure 7

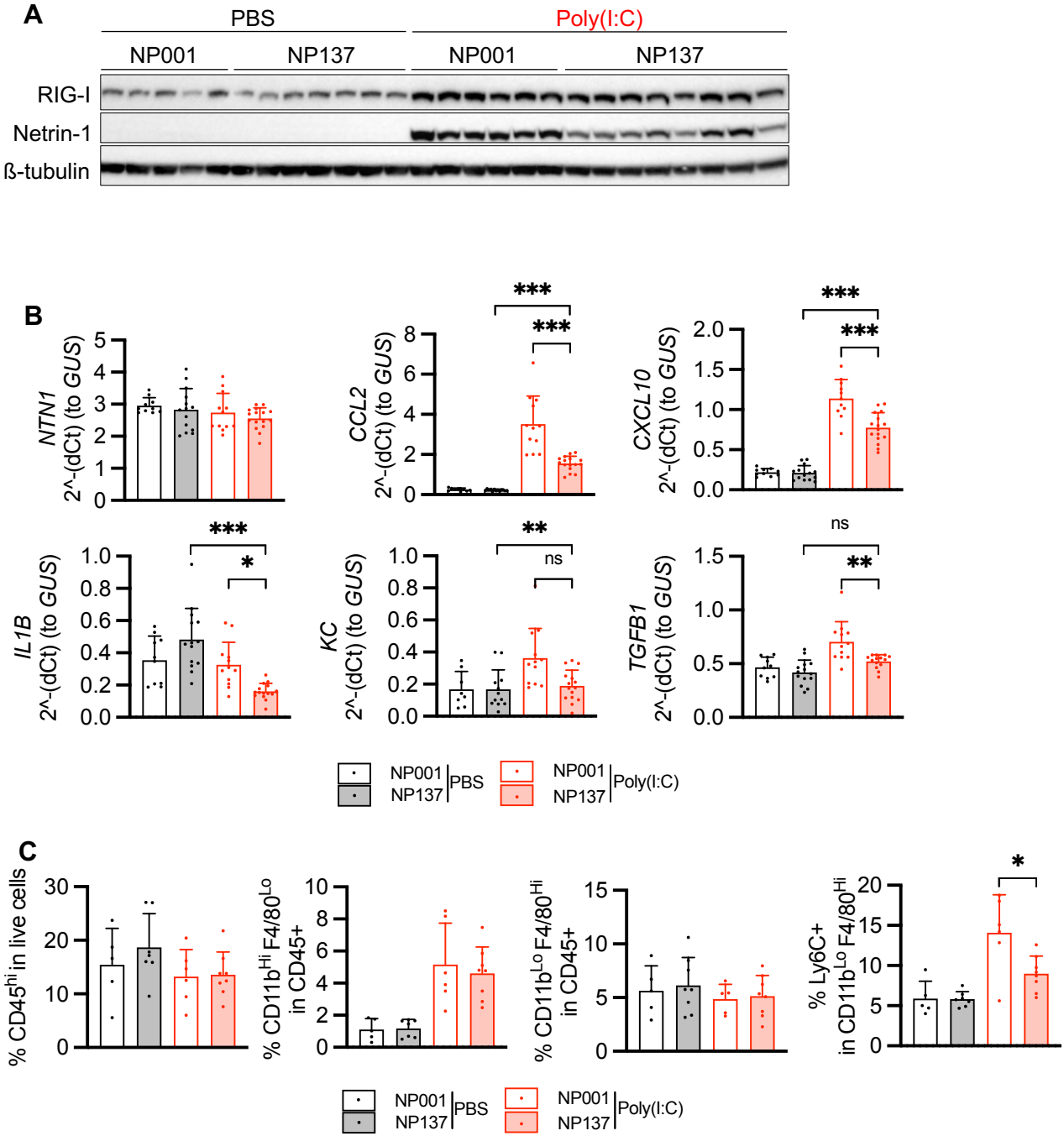
A
PBS
Poly(I:C)
NP001
NP137
NP001
NP137
RIG-I
Netrin-1
ß-tubulin
B
NTN1
CCL2
CXCL10
IL1B
KC
TGFB1
2^-(dCt) (to GUS)
***
**
*
ns
NP001
NP137
PBS
Poly(I:C)
C
% CD45hi in live cells
% CD11bHi F4/80Lo in CD45+
% CD11bLo F4/80Hi in CD45+
% Ly6C+ in CD11bLo F4/80Hi

Figure 8

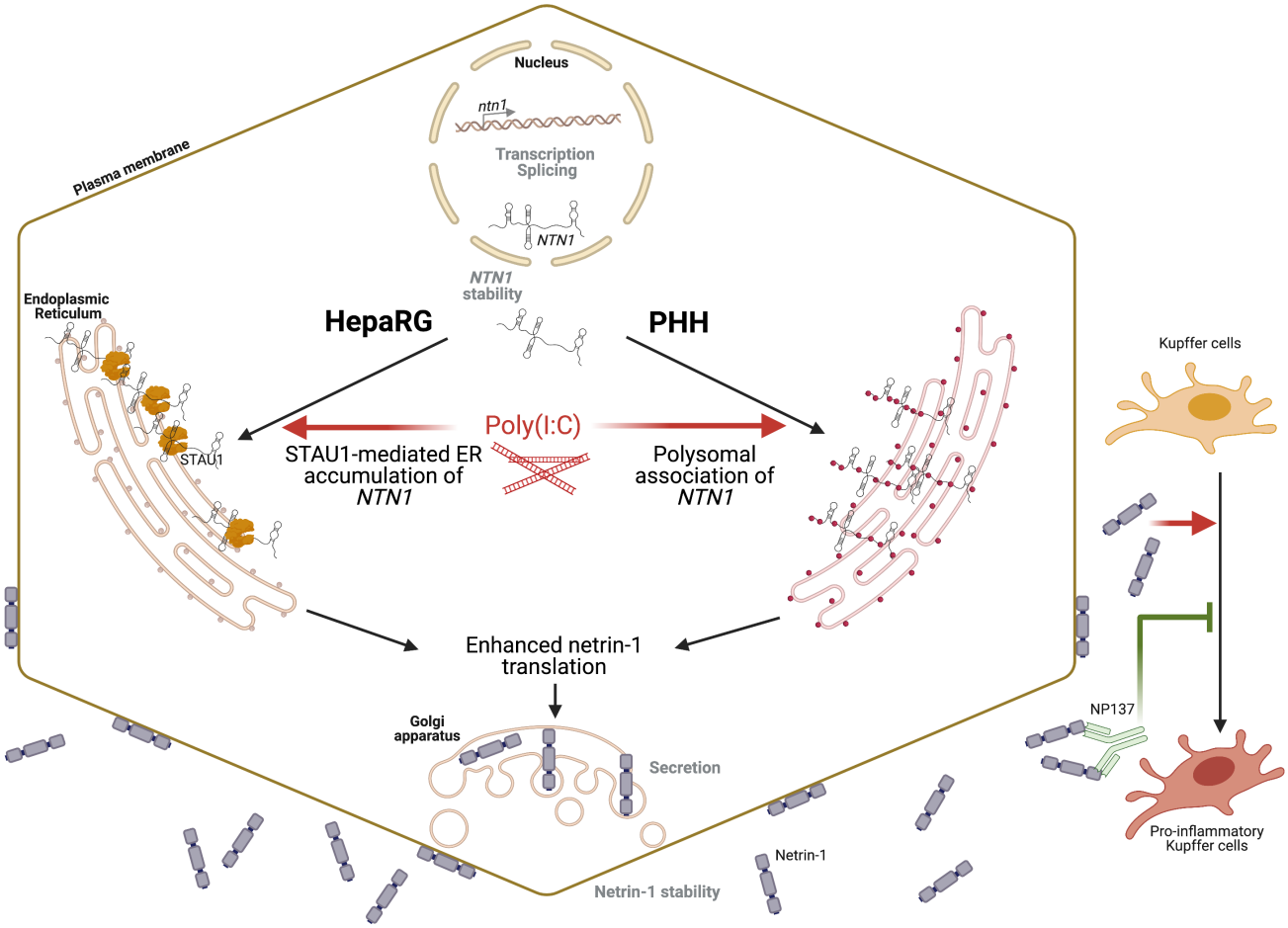
Plasma membrane
Nucleus
ntn1
Transcription
Splicing
NTN1
NTN1
stability
Endoplasmic
Reticulum
HepaRG
PHH
STAU1
Poly(I:C)
STAU1-mediated ER
accumulation of
NTN1
Polysomal
association of
NTN1
Kupffer cells
Enhanced netrin-1
translation
Golgi
apparatus
Secretion
NP137
Pro-inflammatory
Kupffer cells
Netrin-1
Netrin-1 stability

Supplementary figure 1

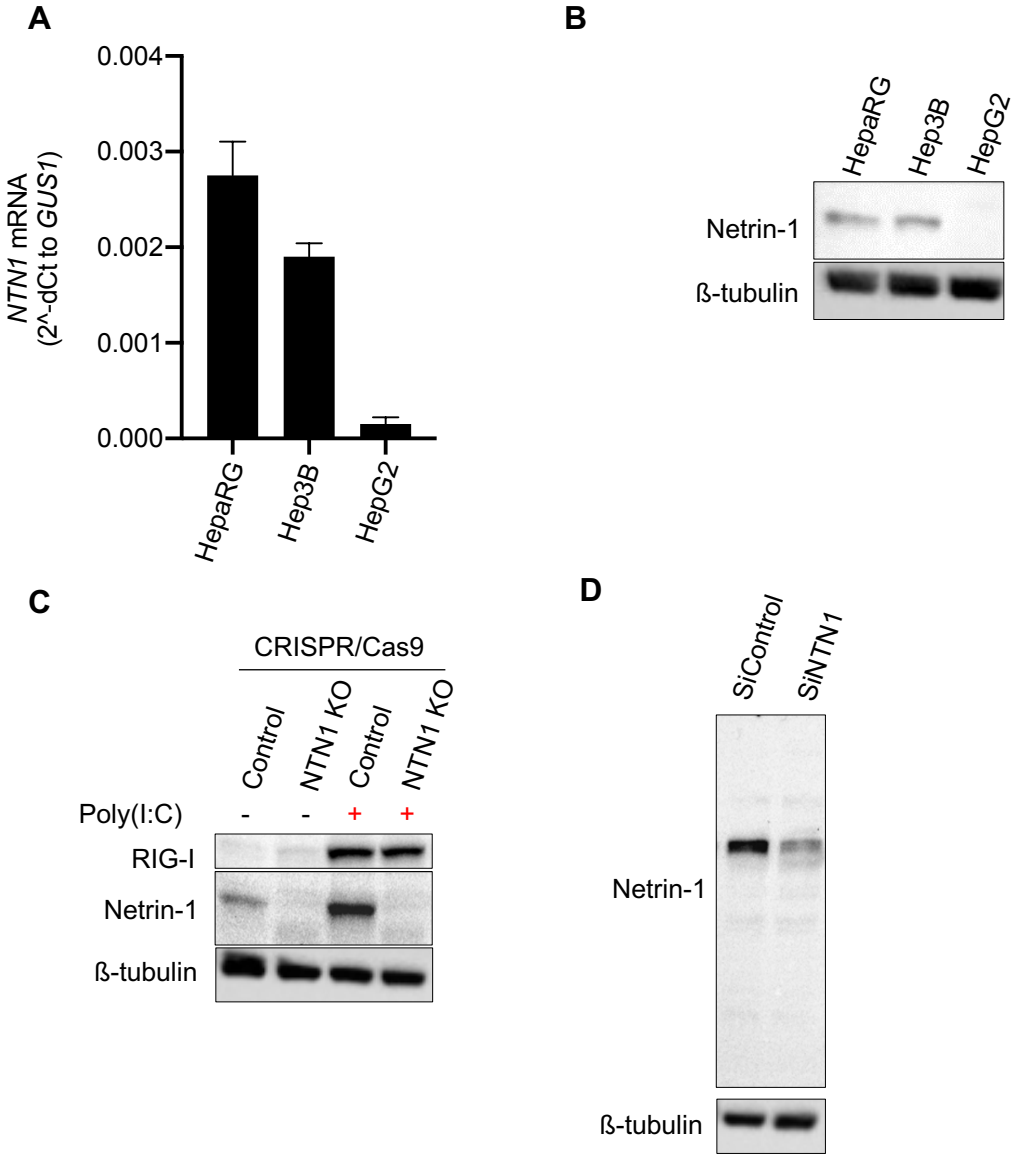

Supplementary figure 2

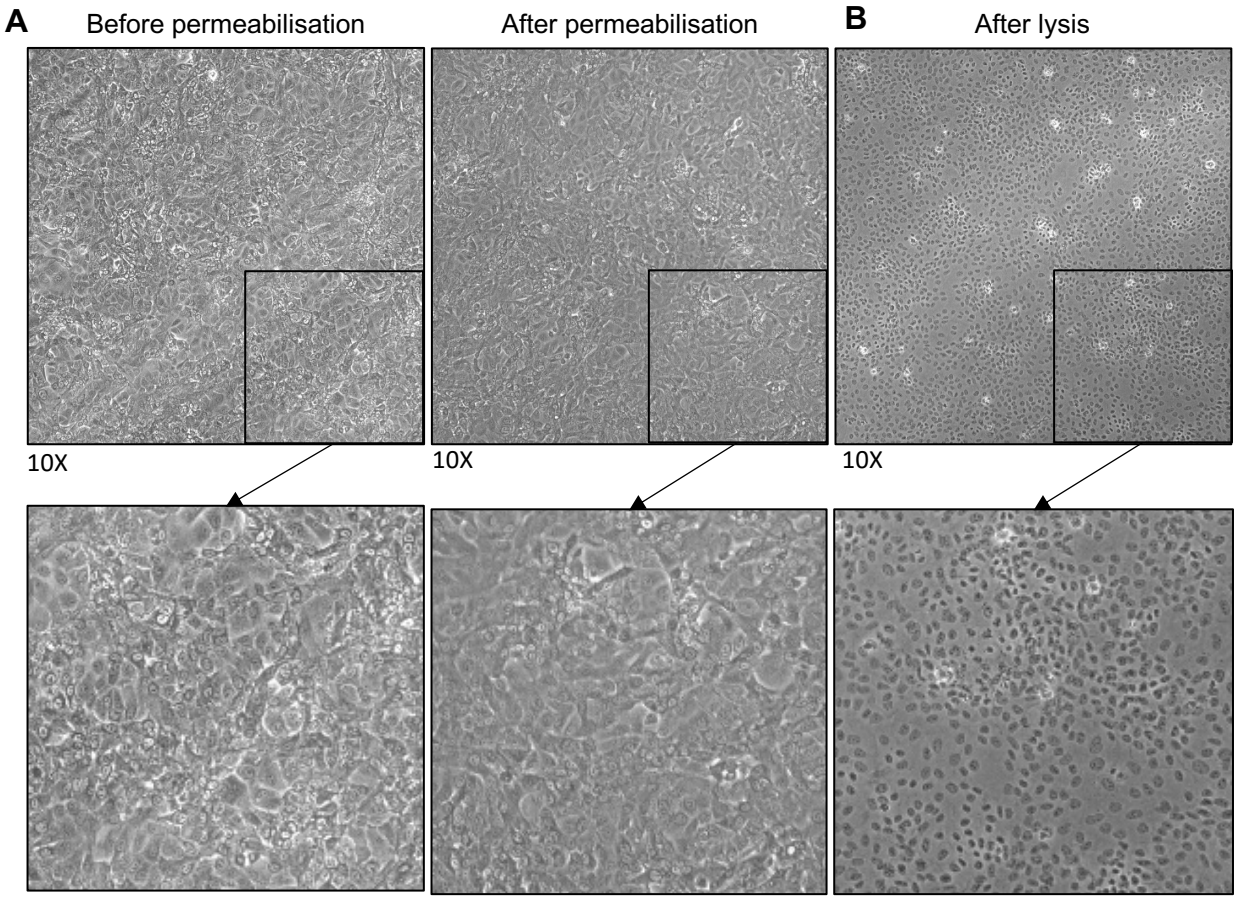

Supplementary figure 3

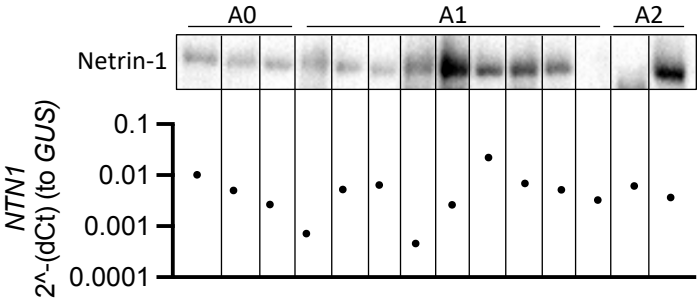

Supplementary figure 4

A

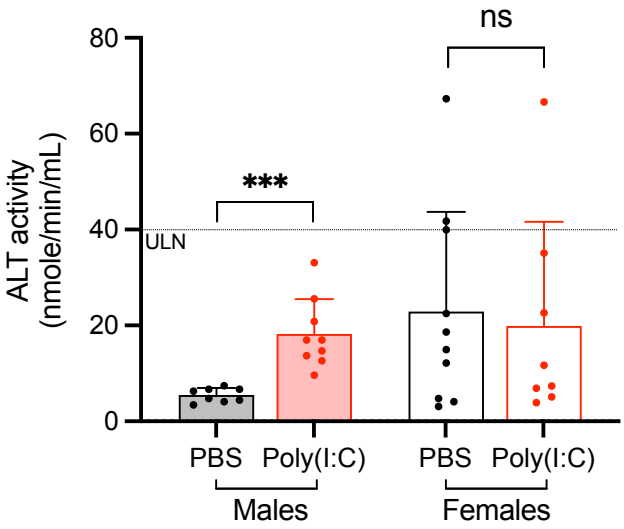

B

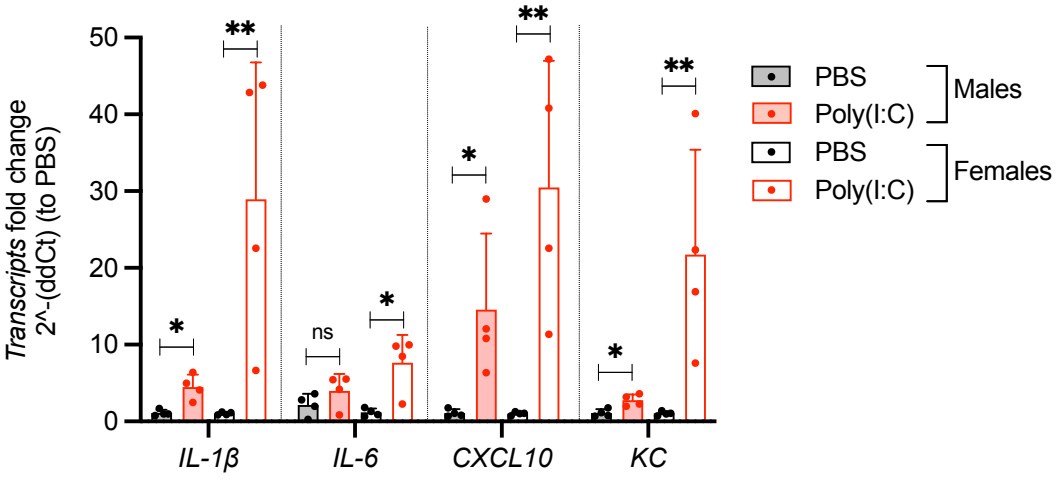

Supplementary figure 5

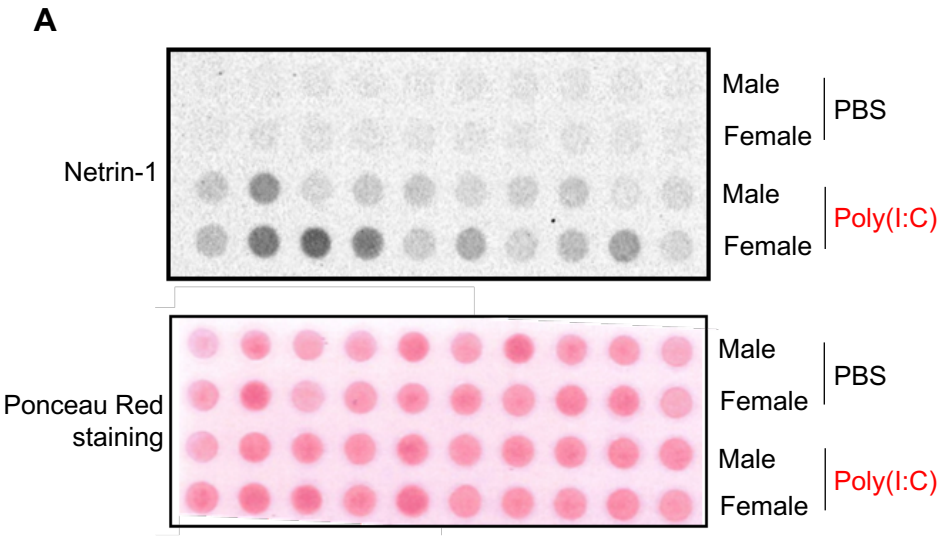

Supplementary figure 6

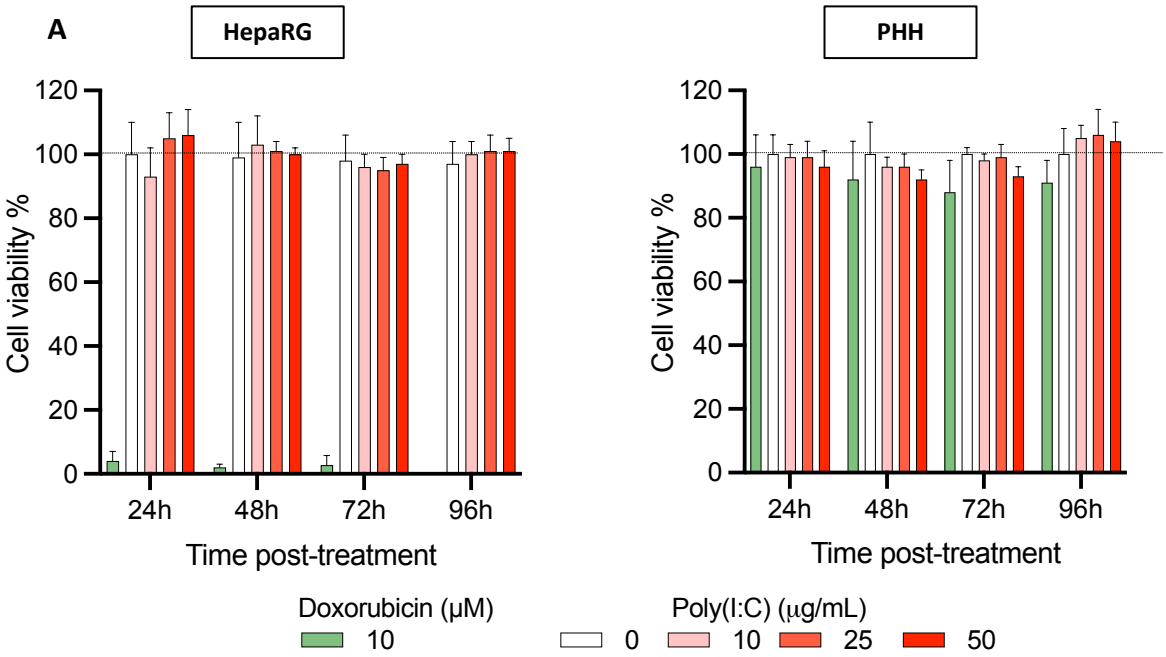

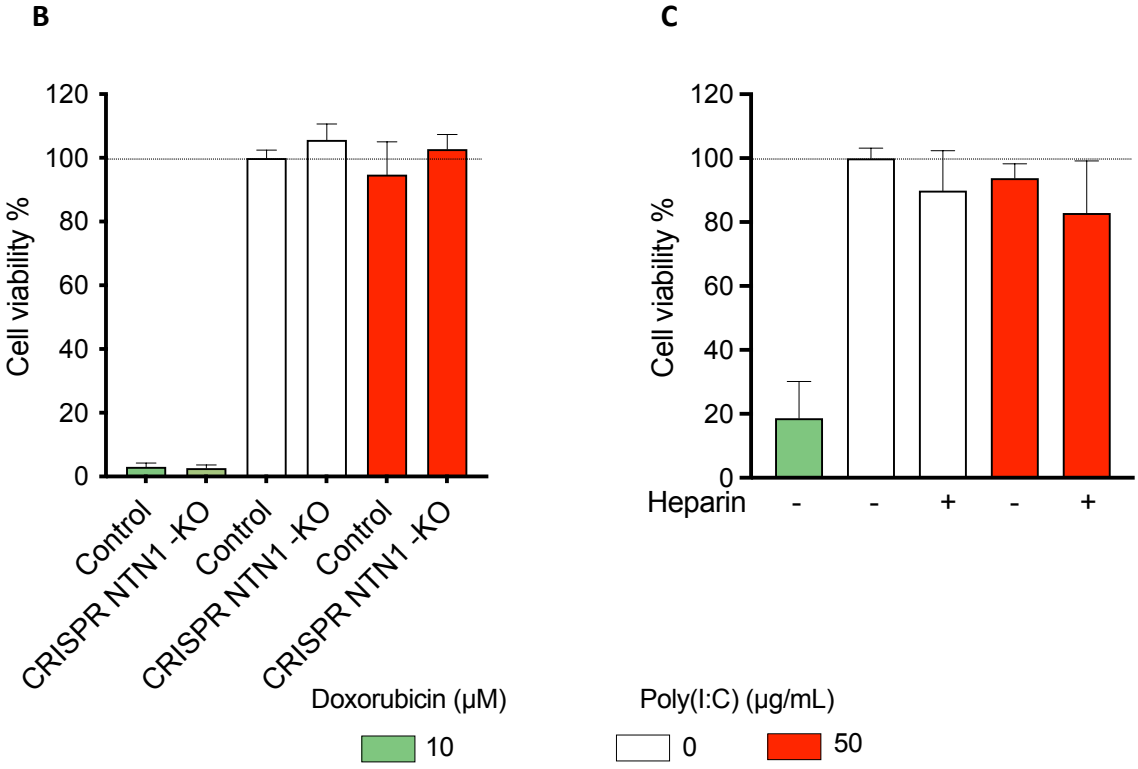

Supplementary figure 7

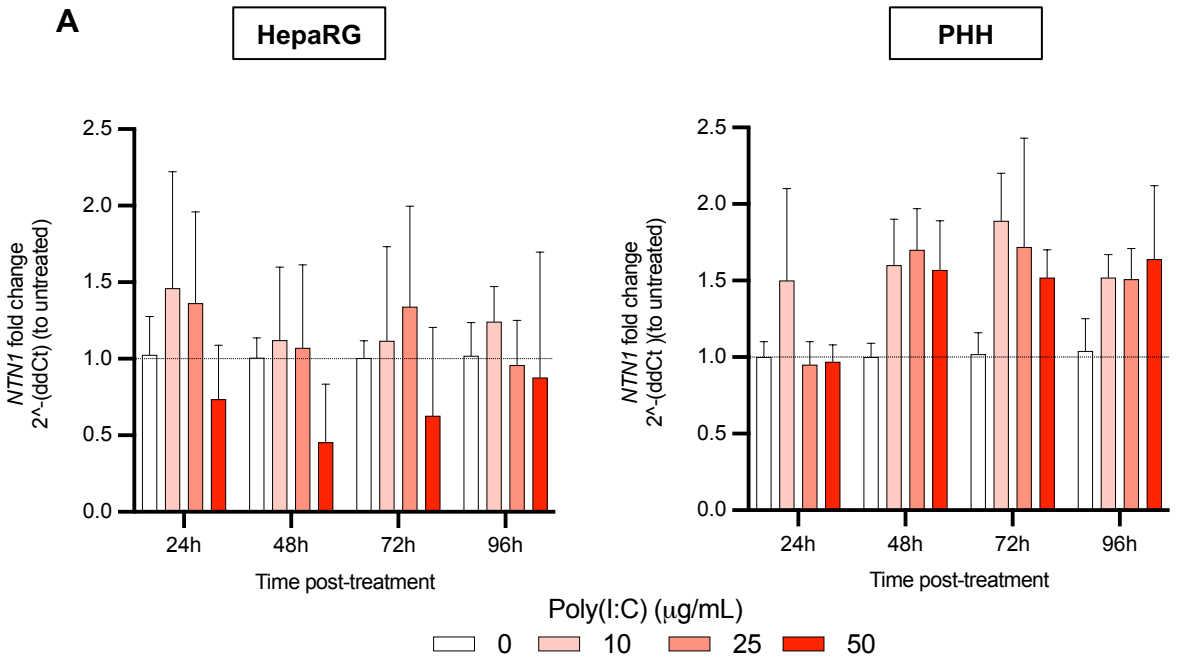

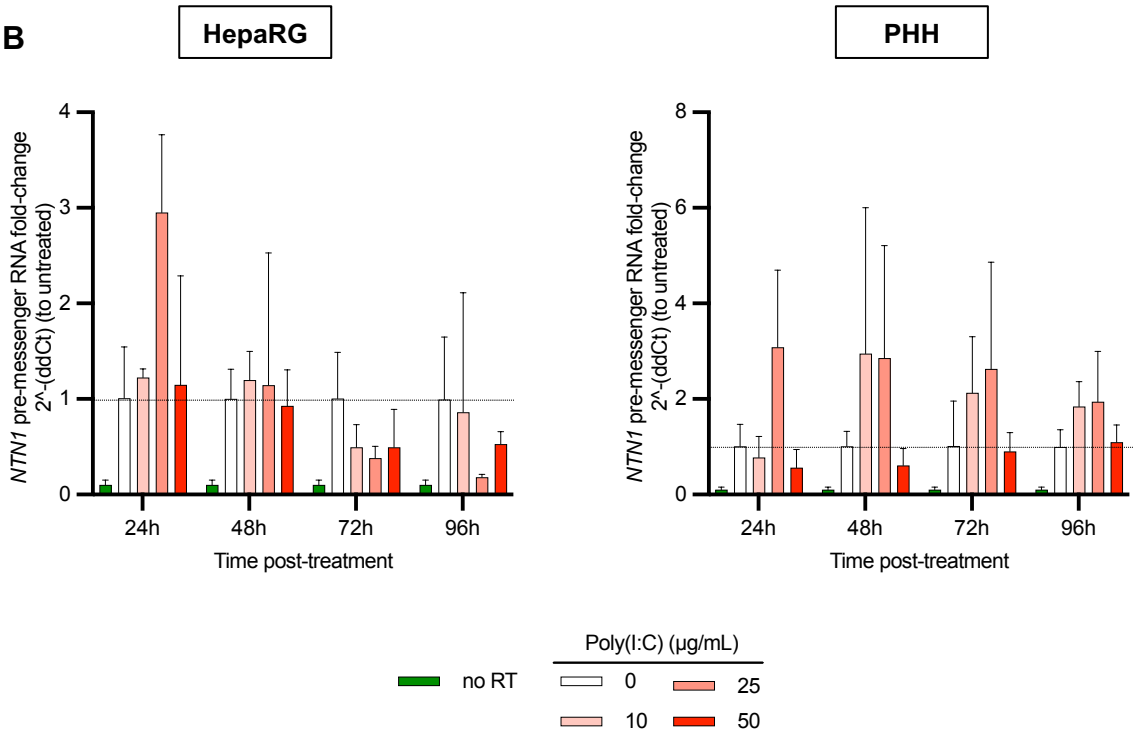

Supplementary figure 8

A

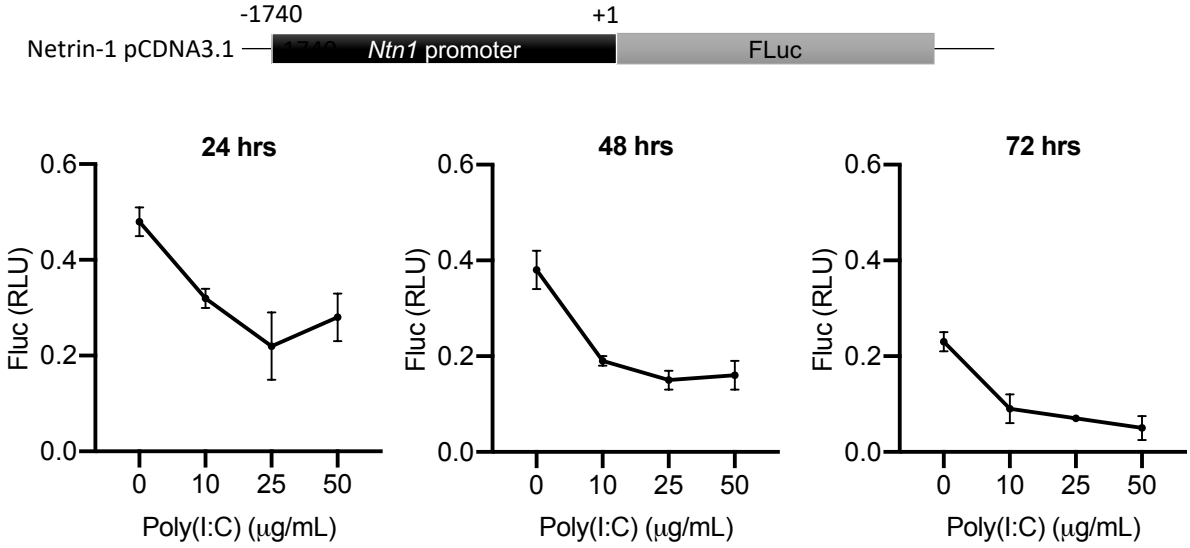

B

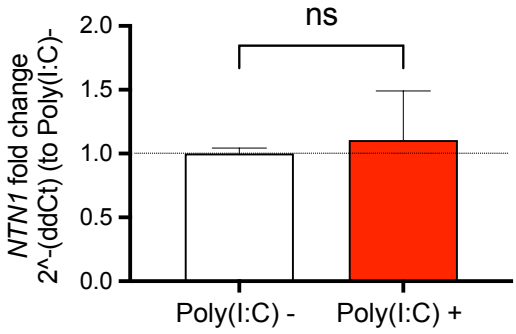

Supplementary figure 9

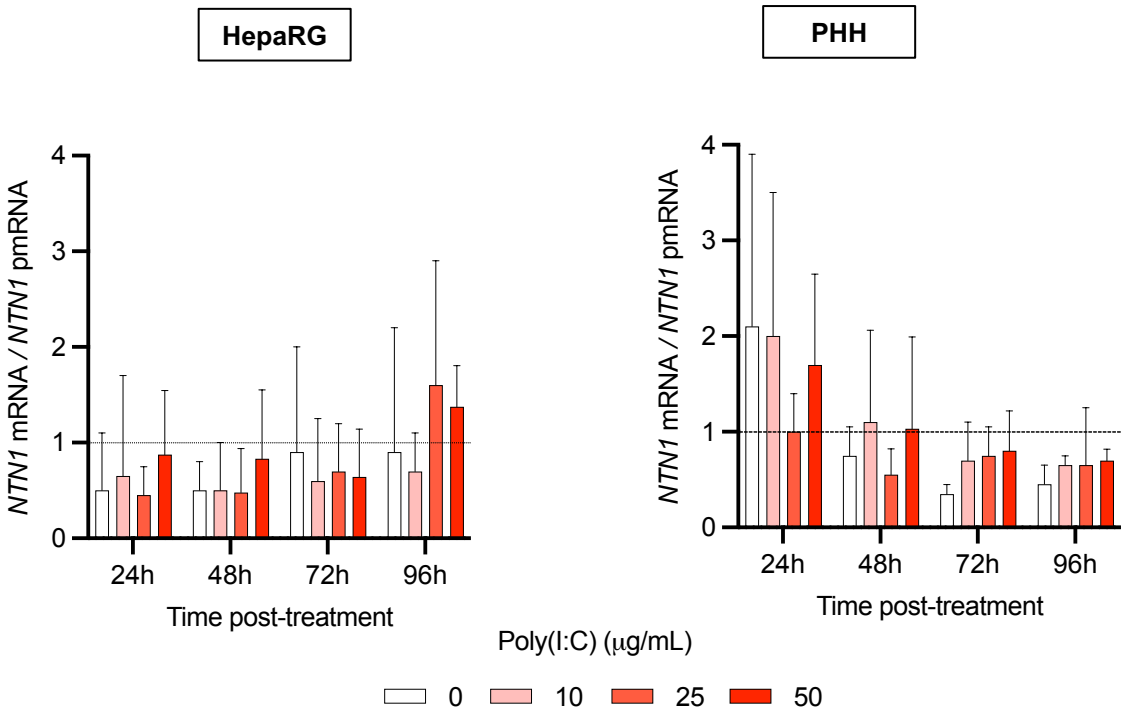

Supplementary figure 10

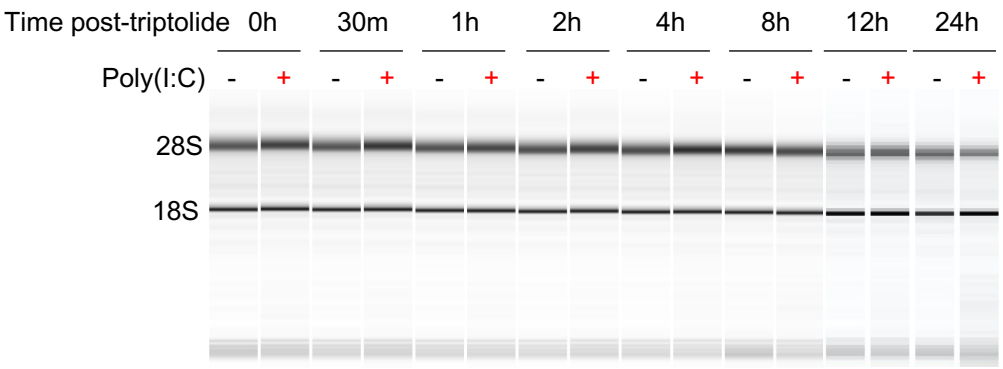

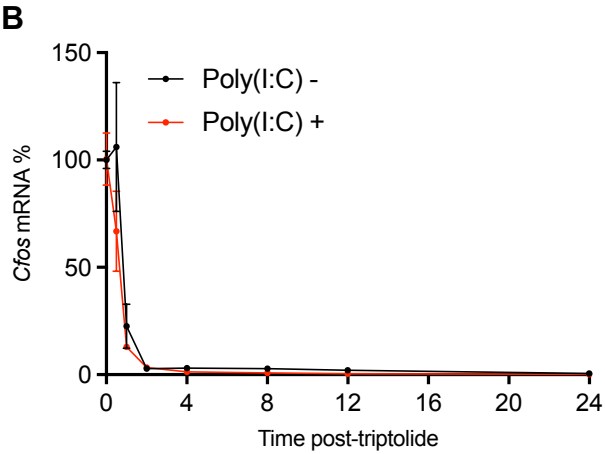

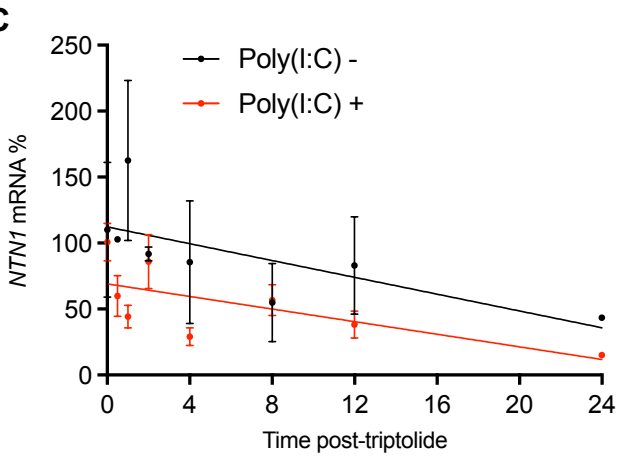

	Poly(I:C)-	Poly(I:C)+
Slope	-3.186 ± 1.255	-2.388 ± 1.030

Supplementary figure 11

A

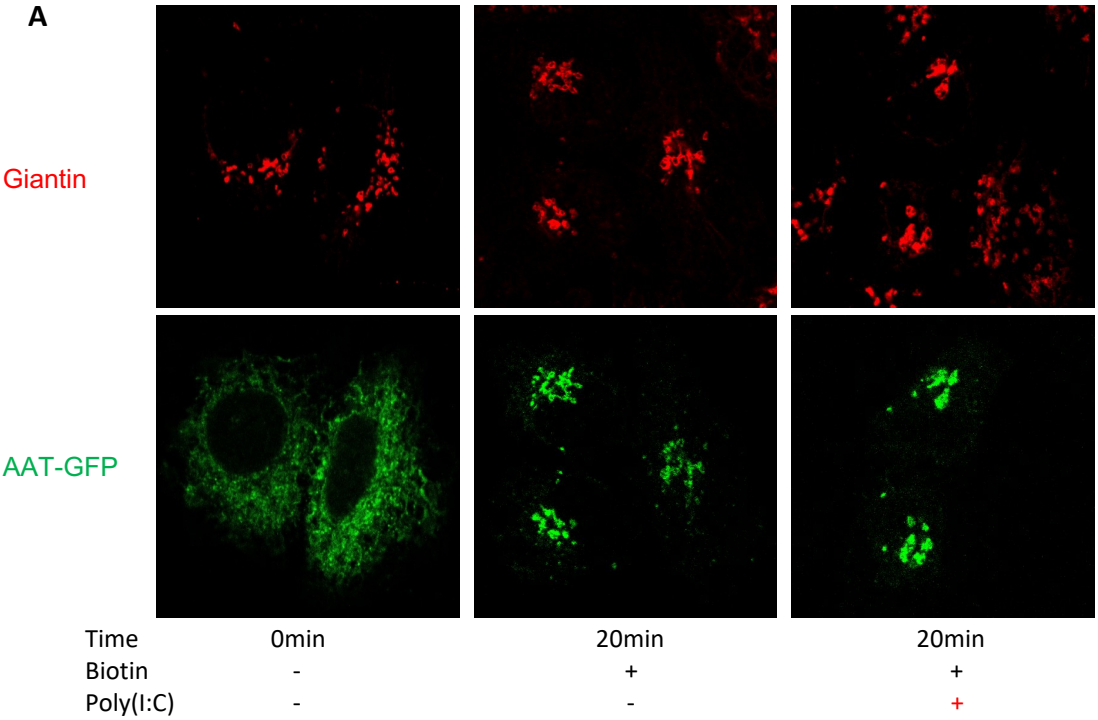

B

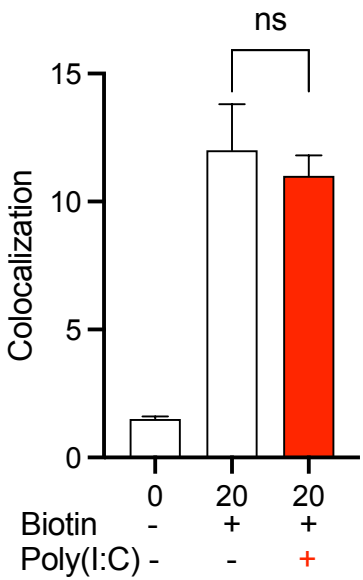

Supplementary figure 12

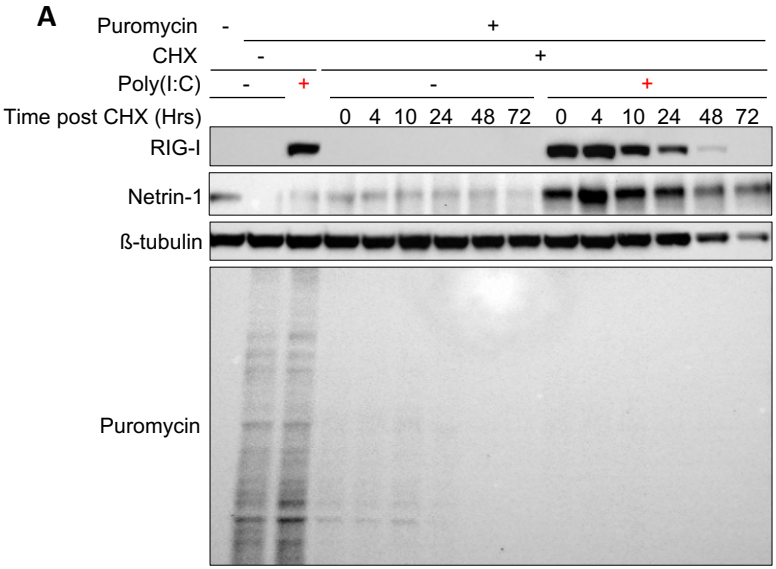

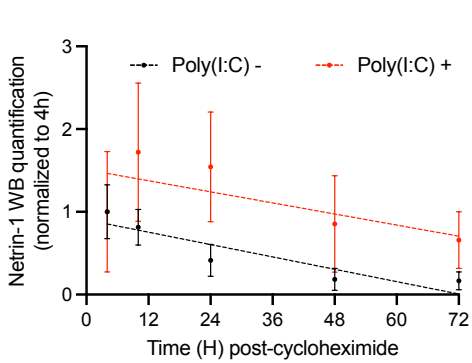

	Poly(I:C)-	Poly(I:C)+
Slope	-0.01245 ± 0.001875	-0.01116 ± 0.005271

Supplementary figure 13

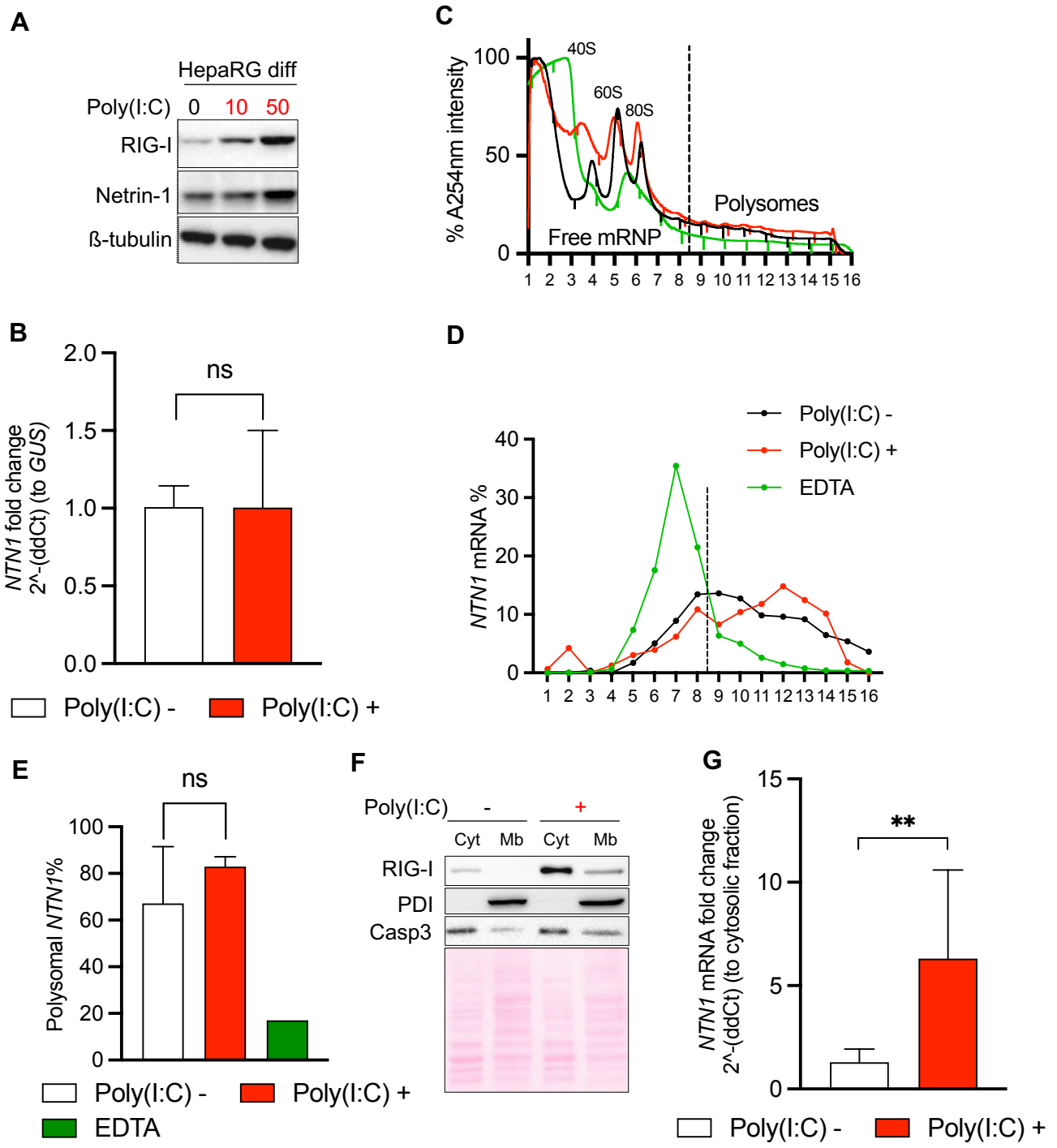

Supplementary figure 14

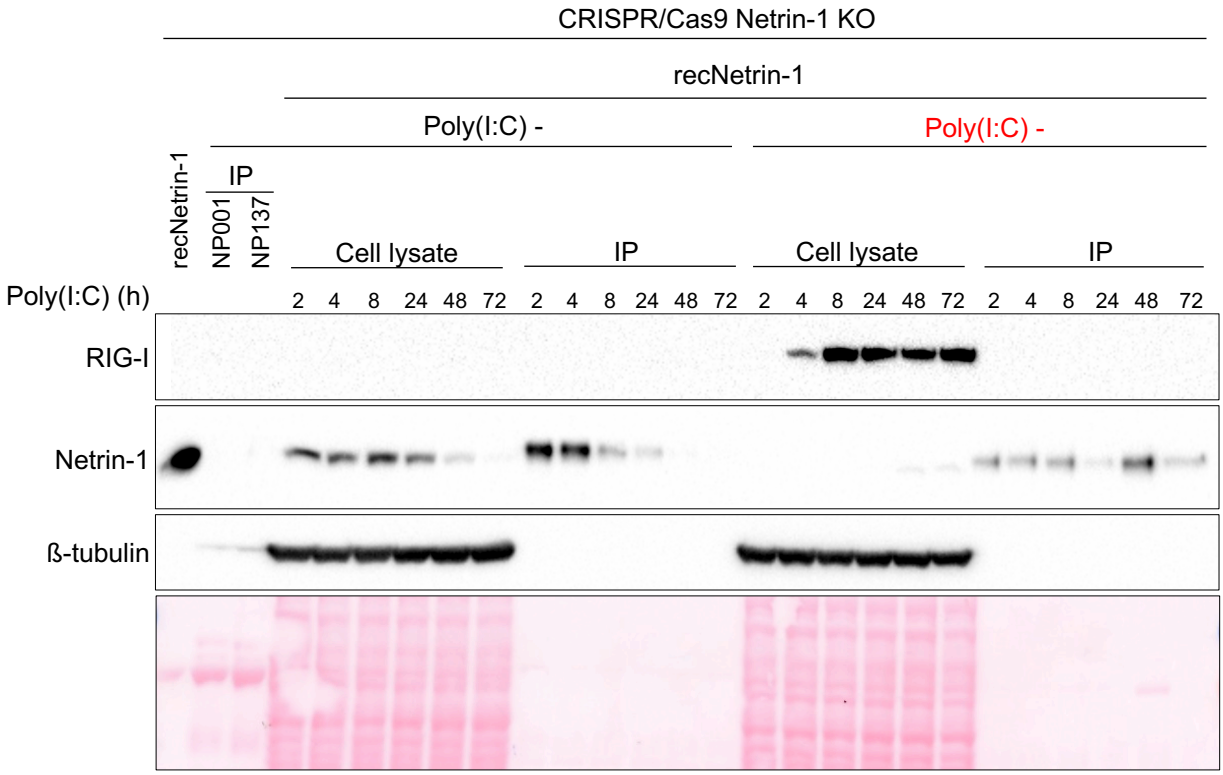
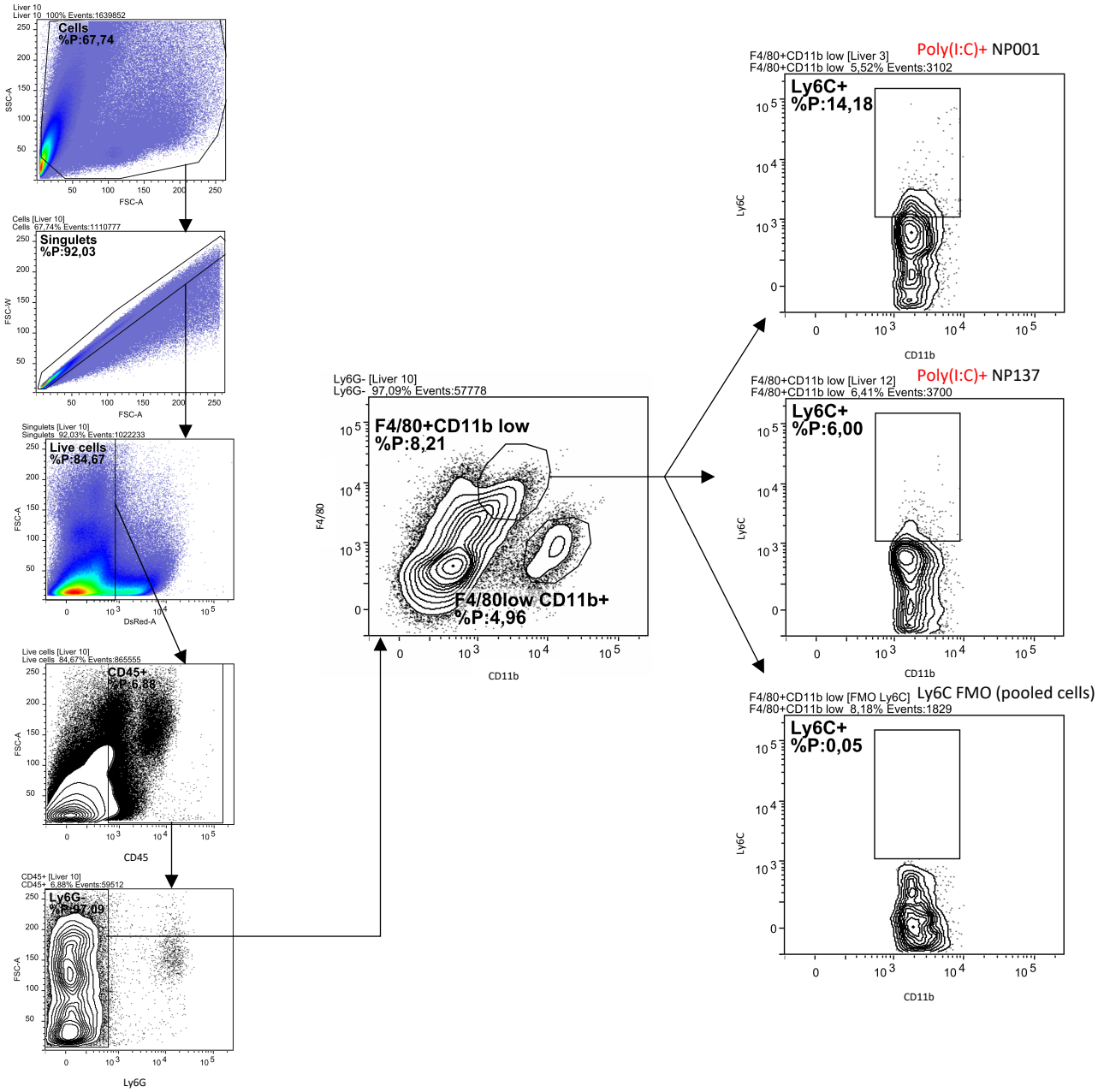
Supplementary figure 15